Direct 17O-isotopic labeling of oxides using mechanochemistry

Chia-Hsin Chen, Emeline Gaillard, Frederic Mentink-Vigier, Kuizhi Chen, Zhehong Gan, Philippe Gaveau, Bertrand Rebière, Romain Berthelot, Pierre Florian, Christian Bonhomme, et al.

Direct ^{17}O-isotopic labeling of oxides using mechanochemistry

Chia-Hsin Chen,[1] Emeline Gaillard,[1] Frédéric Mentink-Vigier,[2] Kuizhi Chen,[2] Zhehong Gan,[2] Philippe Gaveau,[1] Bertrand Rebière,[1] Romain Berthelot,[1] Pierre Florian,[3] Christian Bonhomme,[4] Mark E. Smith,[5] Thomas-Xavier Métro,[6] Bruno Alonso,[1] Danielle Laurencin[1,*]

[1] ICGM, Univ Montpellier, CNRS, ENSCM, Montpellier, France

[2] National High Magnetic Field Laboratory (NHMFL), Florida State University, Tallahassee, FL, USA

[3] Conditions Extrêmes et Matériaux: Haute Température et Irradiation (CEMHTI), UPR 3079 CNRS, Université d'Orléans, 45071 Orléans, France

[4] Laboratoire de Chimie de la Matière Condensée de Paris (LCMCP), UMR 7574, Sorbonne Université, CNRS, 75005 Paris, France

[5] Vice-Chancellor's Office, Highfield Campus, University of Southampton, University Road, Southampton, SO17 1BJ, and Department of Chemistry, Lancaster University, Bailrigg, Lancaster, LA1 4YB, UK

[6] IBMM, Univ Montpellier, CNRS, ENSCM, Montpellier, France

* To whom correspondance should be addressed: danielle.laurencin@umontpellier.fr

Abstract

While oxygen-17 NMR is increasingly being used for elucidating the structure and reactivity of complex molecular and materials systems, much effort is still required for it to become a routine analytical technique. One of the main difficulties for its development comes from the very low natural abundance of oxygen-17 (0.04%), which implies that isotopic labeling is generally needed prior to NMR analyses. However, ^{17}O-enrichment protocols are often unattractive in terms of cost, safety, and/or practicality, even for compounds as simple as metal oxides. Here, we demonstrate how mechanochemistry can be used in a highly efficient way for the direct ^{17}O-isotopic labeling of a variety of s-, p- and d-block oxides which are of major interest for the preparation of functional ceramics and glasses: Li_2O, CaO, Al_2O_3, SiO_2, TiO_2, and ZrO_2. For each oxide, the enrichment step was performed under ambient conditions in less than 1 hour and at low cost, which makes these synthetic approaches highly appealing in comparison to the existing literature. Using high-resolution ^{17}O solid state NMR and Dynamic Nuclear Polarization, atomic-level insight into the enrichment process is achieved, especially for titania and alumina. Indeed, it was possible to demonstrate that enriched oxygen sites are present not only at the surface, but also within the oxide particles. Moreover, information on the actual reactions occurring during the milling step could be obtained by ^{17}O NMR, both in terms of their kinetics and the nature of the reactive species. Finally, it was demonstrated how high resolution ^{17}O NMR can be used for studying the reactivity at the interfaces between different oxide particles during ball-milling, especially in cases when X-ray diffraction techniques are uninformative. More generally, such investigations will be useful not only for producing ^{17}O-enriched precursors efficiently, but also for understanding better mechanisms of mechanochemical processes themselves.

Introduction

Oxygen, as an element, is present in the majority of natural and synthetic materials. It is thus essential to have access to information about the local binding environment around this element to be able to rationalize structure - properties relationships in a variety of systems. Oxygen-17 NMR spectroscopy is one of the most promising spectroscopic techniques for this.[1] Indeed, thanks to the very wide range of variation of ^{17}O NMR parameters, detailed insight into the bulk and surface structure of a variety of materials can be obtained. For example, recent studies have used ^{17}O NMR to elucidate the structure of porous materials like zeolites and metal organic frameworks,[2-5] of mixed metal oxides used as electrode materials,[6-7] or of nanoparticle surfaces.[8-11]

Natural abundance ^{17}O NMR unfortunately suffers from a very poor absolute signal sensitivity, due to the very low abundance of the NMR-active isotope (only 0.04%). This implies that enriching the compounds of interest in ^{17}O is generally necessary to be able to perform high-resolution ^{17}O NMR studies. Until recently, this has actually hampered the large-scale development of ^{17}O NMR spectroscopy, due to the lack of cost-efficient and user-friendly enrichment protocols. Indeed, some of the early labeling schemes employed excessive amounts of expensive ^{17}O-enriched precursors ($H_2{}^{17}O$ or $^{17}O_2$), and/or were experimentally constraining, due to the need to operate under inert atmosphere or at high temperatures, or because of the excessive experimental times (lasting hours or days).[1,12] In the case of oxides, among the different labeling procedures proposed, those based on sol-gel chemistry have found some success for the preparation of ^{17}O-enriched phases. However, they rely on the availability of the metal alkoxide precursors, and also require optimizing not only the hydrolysis and condensation steps, but also the drying step, in order to remove the alcohol by-product from the reaction mixture and produce a dry gel which can be then converted into the metal oxide of interest.[12-16] More recently, affordable and practical ^{17}O-enrichment protocols have been proposed,[3, 17-18] either for the direct labeling of the inorganic or hybrid materials of interest, or for the labeling of the precursors which can then be used for preparing these materials. In both cases, mechanochemistry techniques like ball-milling (BM) have been shown to be particularly attractive.[7, 18]

In ball-milling, mechanical forces are applied to solid particles, in order to mix them efficiently, alter their size and shape, and make them react at their interfaces.[19-20] The addition of small amounts of liquid during the milling process (typically in the order of 0.1 μL/mg of sample) can have a significant impact on the course of the reactions, such as accelerating their speed.[21] This general approach, which is referred to as "liquid assisted grinding" (LAG), served as a basis of the development of new ^{17}O-enrichment schemes. Indeed, we showed that using ^{17}O-enriched water as a liquid-grinding assistant, it was possible to enrich in oxygen-17 a variety of organic and inorganic compounds of synthetic interest, including metal hydroxides like $Mg(OH)_2$, $Ca(OH)_2$ and $Al(OH)_3$.[18] These were then converted into the corresponding metal oxides by heat-treatment under inert atmosphere, leading to the formation of ^{17}O-labeled MgO, CaO and Al_2O_3 (Scheme 1).

Scheme 1. Strategy previously proposed for the ^{17}O-labeling of Mg-, Ca- and Al- oxides, starting from their hydroxides.[18]

The possibility to easily produce ^{17}O-enriched oxides is highly attractive, as these can then be engaged in a variety of reactions using previously established synthetic protocols, to prepare enriched ceramics, glasses, or hybrid organic-inorganic materials. However, in order to further broaden the scope of oxides which can be enriched in ^{17}O using mechanochemistry, it appeared to us necessary to look into synthetic approaches which would not require starting from a hydroxide. Indeed, in contrast to $Mg(OH)_2$, $Ca(OH)_2$ and $Al(OH)_3$, a well-defined and stable form of the starting hydroxide may not be readily available, as is the case for titania and silica. Moreover, the initial labeling step of the hydroxide by LAG proceeds by equilibration in the presence of ^{17}O-enriched water (scheme 1), which is not optimal in terms of enrichment yield, because the by-product formed after full isotopic scrambling will be partially-enriched H_2*O (with the same ^{17}O-labeling level as the final labeled hydroxide). Using oxides as precursors instead of the hydroxides should allow both these issues to be addressed at the same time. Preliminary evidence that oxides could potentially be directly enriched in ^{17}O using LAG was provided in a recent study, in which ^{17}O-labeled alkali transition metal oxides like Li_2MO_3 (M = Mn, Ru) were synthesized by performing an initial LAG step on non-enriched oxide precursors in the presence of ^{17}O-enriched water, followed by a heat-treatment at high temperature.[7] However, no detail regarding the mechanisms by which the isotopic labeling was occurring was proposed, making it difficult to determine at what moment of the reaction the enrichment had taken place, and how to adapt this strategy to other materials systems in order to achieve optimal labeling for high resolution ^{17}O NMR.

In this article, we study the reactivity of a selection of oxides under LAG using ^{17}O-labeled water, with the overall goal of producing ^{17}O-enriched compounds of synthetic interest for the elaboration of advanced functional materials. First, an improved strategy for preparing Ca*O will be described, calcium oxide being of interest for the elaboration of bioceramics and bioglasses. Its extension to the synthesis of Li_2*O is also presented, this precursor being important for preparing lithium-based batteries and ion-conducting glasses. Then, the direct labeling of four widely-used oxides of different composition and crystallinity (silica, alumina, titania and zirconia) will be discussed, providing insight into the isotopic enrichment process using high-resolution ^{17}O NMR and DNP (Dynamic Nuclear Polarization) analyses. Besides the interest for direct and efficient ^{17}O-labeling, it will be shown how our approach offers new opportunities for understanding mechanochemical processes at the atomic level.

Results and discussion

1/ Improved LAG approach for the ^{17}O-labeling of s-block metal oxides

We first focused on improving the labeling strategy we had previously proposed for enriching calcium oxide.[18] More specifically, in order to avoid the initial equilibration step (scheme 1) and to achieve a better enrichment level of the intermediate hydroxide, we started from the non-labeled oxide CaO, and hydrolyzed it by mechanochemistry to produce Ca(*OH)$_2$ (scheme 2). The idea here is that all the ^{17}O label introduced as H$_2$*O during the LAG step reacts with CaO to form the ^{17}O-enriched hydroxide.

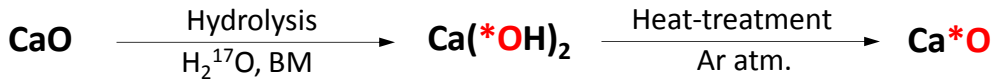

Scheme 2. Alternative strategy proposed here for the ^{17}O-labeling of Ca oxide.

The BM conditions required to perform the hydrolysis step were initially tested using non-labeled water, by analyzing the reaction medium by powder X-ray diffraction (PXRD). It was found that after 1 hour milling of CaO at 25 Hz in the presence of 1 equivalent of water, complete conversion into the hydroxide phase occurred. Using these synthetic conditions with ^{17}O-enriched water, ^{17}O-labeled Ca(*OH)$_2$ was then obtained, as shown by PXRD (Figure 1a) and ^{17}O Magic Angle Spinning (MAS) solid state NMR (Figure 1b, top). This phase could then be transformed into enriched Ca*O by heat treatment under an inert atmosphere (Figure 1b, bottom).

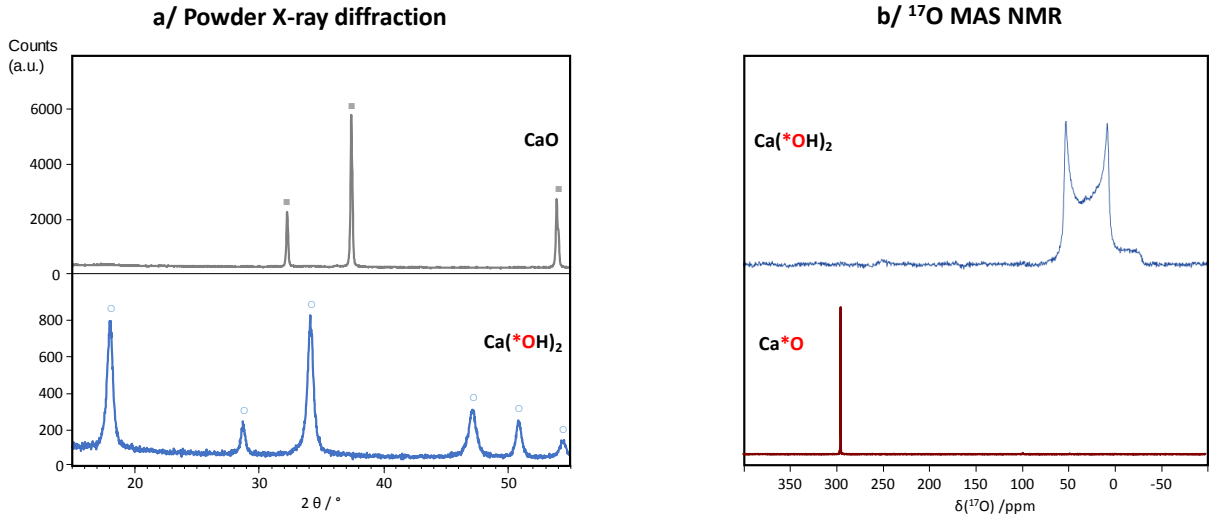

Figure 1. a/ PXRD analyses before and after LAG: CaO precursor obtained after heat-treatment of commercial Ca(OH)$_2$ (top), and enriched phase recovered after LAG in the presence of H$_2$*O (bottom). "■" and "○" symbols correspond to the diffraction peaks expected for CaO (ICSD # 163628) and Ca(OH)$_2$ (ICSD #15471), respectively; **b/** ^{17}O solid state NMR spectra of ^{17}O-enriched Ca(*OH)$_2$ (prepared by LAG of CaO using H$_2$^{17}O) and Ca*O (obtained after heat-treatment of Ca(*OH)$_2$). These ^{17}O MAS NMR spectra are in agreement with previous measurements at this magnetic field.[18]

Based on the above, it is clear that direct conversion of oxides like CaO into their hydroxides can be achieved by BM in the presence of stoichiometric amounts of ^{17}O-enriched water, which is an improvement for the production of labeled hydroxides like $Ca(*OH)_2$.[18] Using a similar approach, the labeling of other s-block oxides like Li_2O could be achieved, which provide attractive alternatives in comparison to existing protocols,[22-23] as discussed in supporting information S1. As detailed below, the extension of this type of approach to oxides of the p- and d- blocks was then studied, in order to expand the scope of precursors which could be enriched by this technique.

2/ ^{17}O-labeling of p and d-block oxides using LAG

2a/ Enrichment of SiO_2, Al_2O_3, TiO_2 and ZrO_2: structural analyses after 1 hour LAG

Silica, alumina, titania and zirconia were selected for the ^{17}O labeling tests on p- and d-block oxides, due to their numerous usages for the preparation of functional materials. For each of these phases, the starting materials were commercially available porous samples with relatively high surface areas (all above 80 m^2/g), as this was expected to favor surface-reactions with the enriched water during BM. Based on scanning electron microscopy (SEM) and PXRD analyses, each precursor was initially composed of agglomerated nanoparticles of ~10 to 20 nm diameter, but with different crystallinity. Indeed, while the silica precursor was fully amorphous, the three others gave diffraction peaks in XRD, which could be assigned to the anatase phase for titania, to the monoclinic polymorph for zirconia, and to a mixture of γ and δ polymorphs for alumina (see Figure 2, inserts).

Each compound was milled in presence of stoichiometric amounts of ^{17}O-enriched water, for durations up to 1 hour. The initial LAG conditions were set such that 1 equivalent of "MO_y" (y = 2 for M = Si, Ti, Zr, and y = 3/2 for M = Al) was reacted with 1 equivalent of H_2*O, as a means to minimize losses of H_2*O, if the BM hydrolysis reaction were to be incomplete. Milled samples were characterized by PXRD, nitrogen adsorption/desorption isotherms, SEM, energy dispersive X-ray spectroscopy (EDXS), and ^{17}O MAS NMR (see Figure 2 and Figures S2 to S5).

After 1 hour of LAG, no new phase was observed by PXRD, and the diffractograms of all phases were essentially the same as the ones recorded before milling (Figure 2, inserts). In SEM, the presence of agglomerated nanoparticles could still be observed, without any significant change in particle size, except in the case of silica, for which nanoparticles appeared to have merged into forming larger entities. More striking differences were found in the nitrogen adsorption-desorption isotherms of all oxides before and after milling (Figures S2 to S5), due to changes in surface area and/or pore geometry. In the case of silica, a decrease in porosity was observed (the surface area being reduced by a factor of ~ 3), while in the case of alumina, the main change concerned the pore geometry (as the surface area remained essentially the same as before milling). For titania and zirconia, the differences in the isotherms revealed that both a reduction in surface area and a change in pore geometry had occurred, pointing to significant surface-reconstruction taking place during the

milling. In order to understand the changes in texture of the different oxides, high-resolution NMR experiments were performed.

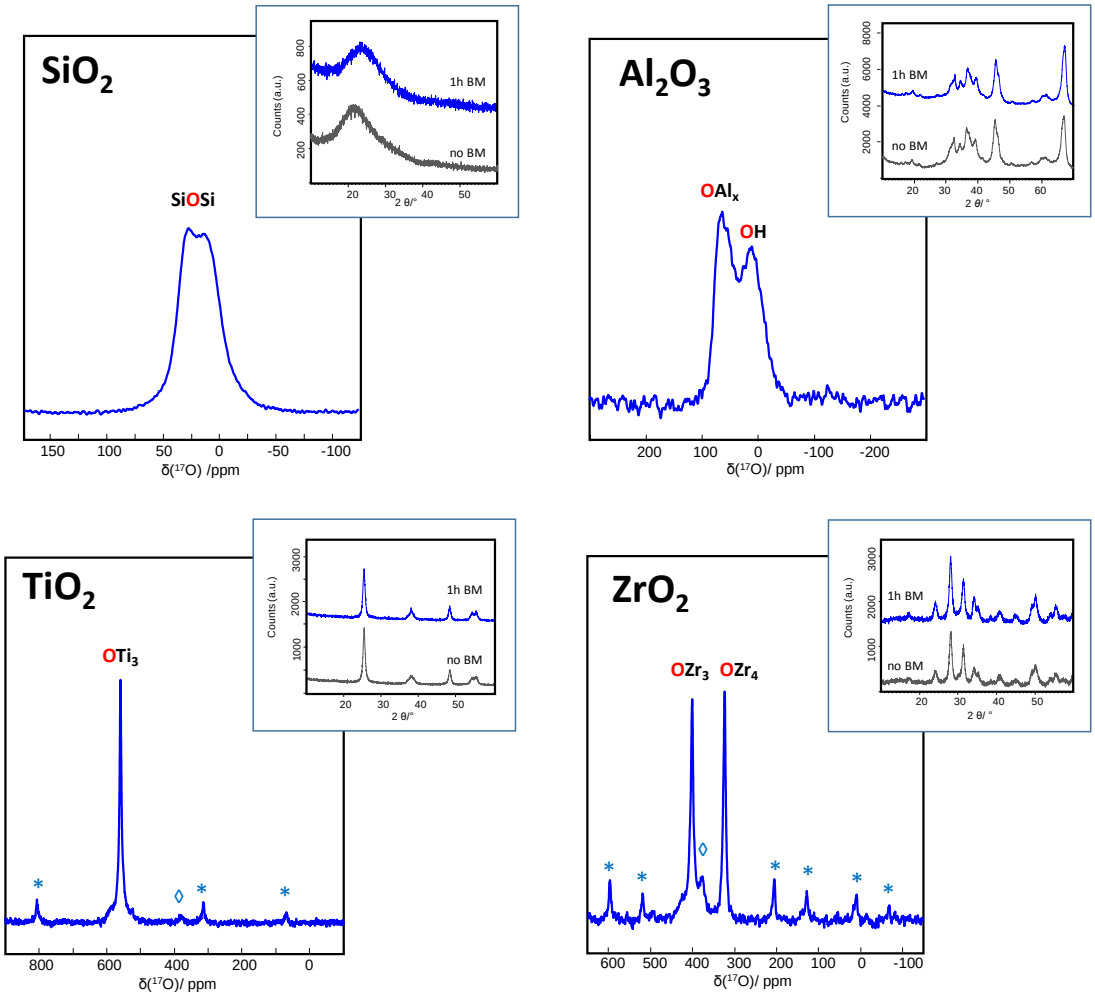

Figure 2. ^{17}O MAS NMR spectra recorded at 14.1T for the SiO_2, Al_2O_3, TiO_2 and ZrO_2 phases, after 1 hour BM in presence of $H_2{}^{17}O$ (followed by drying under vacuum at room temperature). Inserts show the PXRD patterns before (grey) and after (blue) 1 hour of BM in presence of $H_2{}^{17}O$. * symbols correspond to spinning sidebands, and ◊ symbols to the zirconia rotor background signal (see Figure S6a). All NMR acquisition conditions are provided in Supporting Information (Table S1).

All four materials were analyzed by ^{17}O solid state NMR (Figure 2). The spectra obtained show that in all cases the labeling was successful. Indeed, for each oxide, ^{17}O NMR resonances attesting of the formation of a significant proportion of $*OM_x$ environments (M = Si, Al, Ti, Zr) were observed. In the case of silica, the observed quadrupolar lineshape is consistent with enriched siloxanes (Si-*O-Si), as shown by the fit of the ^{17}O MAS spectrum (Figure S7).[1, 24-25] Concerning alumina, two broad resonances are observed, the high-frequency contribution (centered at ~60 ppm at 14.1T) coming from various $*OAl_x$ environments (x = 3, 4),[12, 25-26] while the other originates from *OH groups, as further discussed below. In the case of titania, the main ^{17}O resonance is centered at ~560 ppm, which corresponds to the $*OTi_3$ environments of anatase.[27-28] Regarding zirconia, two sharp resonances are observed, which are centered at 325 and 403 ppm, and correspond to the $*OZr_4$

and *OZr_3 environments of the monoclinic form.[14, 27, 29] For the latter two phases, it is particularly noteworthy that the main ^{17}O NMR resonances detected are those of crystalline environments of titania (anatase form) and zirconia (monoclinic form). Hence, although XRD had not revealed any strong changes during the LAG step, ^{17}O NMR shows that a significant restructuring of the four oxides actually occurs, which leads to the breaking/formation of multiple M-O bonds, and eventually results in a significant proportion of enriched *OM_x core-like environments.

The ^{17}O solid state NMR data also reveals that the overall ^{17}O-enrichment level is high (see Figure S6b for comparison with natural-abundance data). More quantitative analyses were carried out on the silica and titania samples using surface ion mass spectrometry (SIMS), in order to determine the absolute enrichment after the LAG step. Measurements were performed on ^{18}O-enriched samples, which were prepared using a similar procedure as above, but with 97% ^{18}O-labeled water to achieve better quantification by SIMS. Under these conditions, given that 1 equivalent of H_2*O is reacted with 1 equivalent of MO_2 (M = Si, Ti), the maximum enrichment was expected to be ~ 32% (*i.e.* ~ 97/3) in the case of complete isotopic scrambling of the oxygen sites during the $H_2{}^{18}O$-LAG. After 1 hour LAG (followed by drying at room temperature under vacuum), the ^{18}O-enrichments determined by SIMS were of 27% for silica and 15% for titania. This demonstrates that the isotopic scrambling was indeed nearly complete for silica under the milling conditions used here, but that a higher enrichment level is potentially achievable for titania. From a more general perspective, considering that the natural abundance of ^{17}O is only 0.04%, these analyses confirm that high enrichment levels of oxides can be easily reached by LAG in just 1 hour, using stoichiometric amounts of enriched H_2*O.

2b/ Insight into the labeling mechanisms: NMR analyses after different LAG times

Given that the source of ^{17}O is enriched water, it is reasonable to propose that part of the labeled *OM_x sites have formed by condensation reactions involving intermediate M-*OH species (M = Si, Al, Ti, Zr). Additional multinuclear NMR analyses at different milling times were thus performed on each of the oxides to gain more insight into the enrichment mechanisms. The most complete studies were carried out on alumina and titania, as described below.

Alumina

Quantitative ^{17}O NMR analyses were performed on alumina phases recovered after different LAG times (between 5 minutes and 1 hour). In all cases, two main resonances were observed at 14.1T, which were centered at ~ 9 and 60 ppm. As mentioned above, the higher frequency signal corresponds to *OAl_x environments, and its intensity was found to gradually increase with the milling time (see Figures 3a-b). This is all the more interesting that no significant changes could be observed for these samples in the X-ray diffraction patterns, nor in the ^{27}Al MAS and $^{27}Al\{^1H\}$ CPMAS NMR spectra (aside from the appearance of a very weak Al^V signal after 1h BM, as shown in Figure S8). These

observations confirm that ^{17}O NMR can provide unique insight into both structural and kinetic aspects of the bonding-rearrangements occurring at the atomic level during ball-milling for this system.

The broad low frequency signal (centered at ~9 ppm) is consistent with labeled *OH groups. Given that both Al_x-OH species and H_2O molecules can potentially be found in this chemical shift range at 14.1 T,[25-26, 30-32] additional characterizations were performed at ultra-high magnetic field (35.2 T), to reduce the effect of second-order quadrupolar broadening[12] and discriminate better the *OH and H_2*O species. When comparing the 1D MAS spectrum at 35.2T to data reported in the literature,[4, 25, 31-32] it appears that few ^{17}O-enriched water molecules are likely to be present, meaning that the majority of enriched *OH groups correspond to Al_x-*OH species (Figure 3c). In order to achieve higher resolution, complementary analyses were performed, using the ^{17}O multiple quantum MAS (MQMAS) sequence.[33] This allowed the Al_x-*OH sites to be more clearly separated from the *OAl_x ones (Figure 3d, dashed circles). Moreover, it revealed a significant distribution in the ^{17}O chemical shifts for both types of sites, which each span more than 30 ppm. This means that there are several different *local* environments for the enriched oxygen sites, possibly because of variations in the H-bond network around them, and/or in the number and type of Al^{3+} cations to which they are bound. To analyze this in more detail, additional high-resolution ^{1}H-^{17}O and ^{27}Al-^{17}O heteronuclear correlation experiments were carried out.

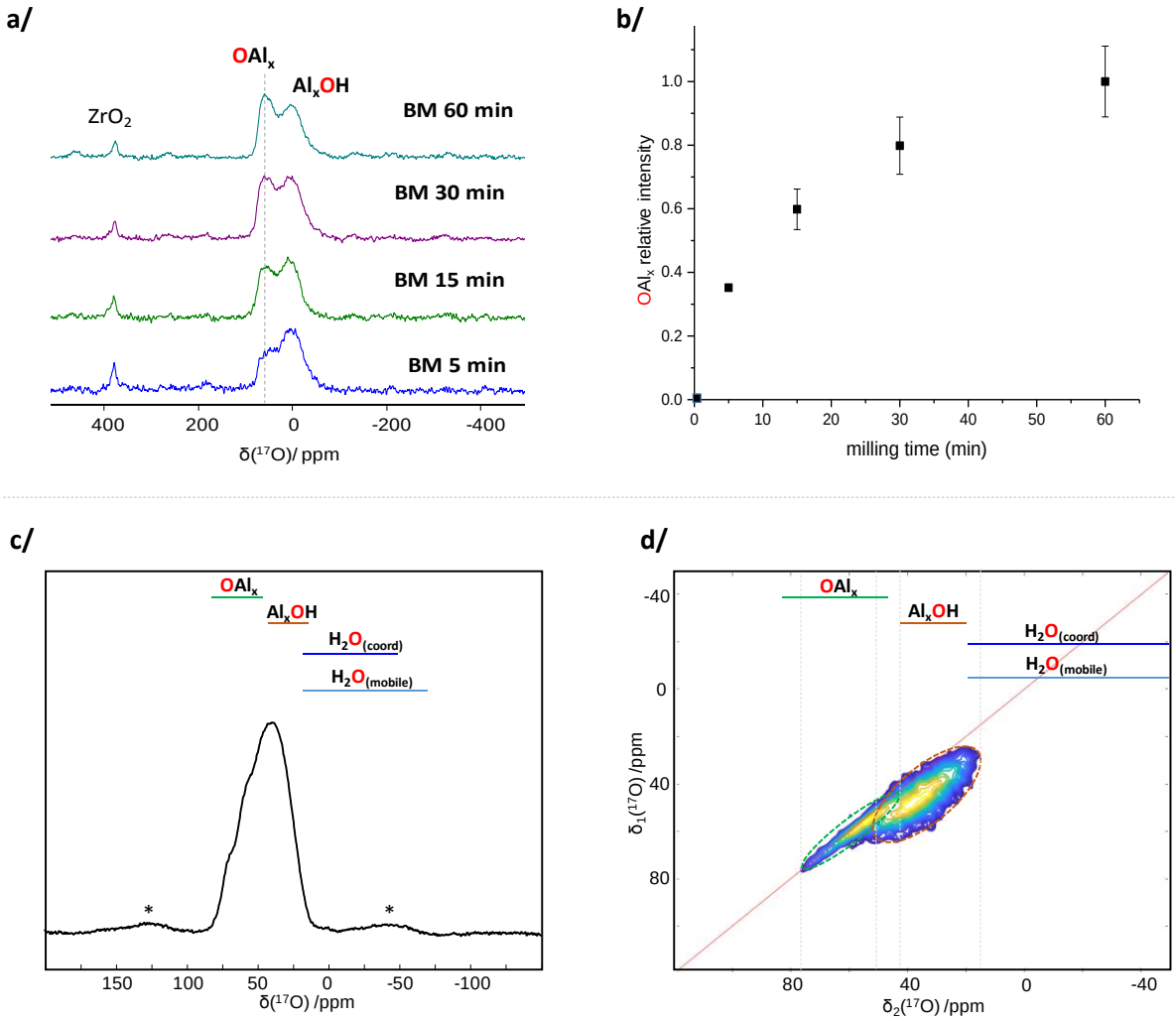

Figure 3. a/ Quantitative single pulse ^{17}O MAS NMR spectra, recorded at 14.1 T for Al_2O_3 phases obtained after different milling times in the presence of $H_2{}^{17}O$, followed by drying under vacuum at room temperature (all spectra were acquired over 18 h, using a $\pi/12$ excitation pulse and a recycle delay of 16s). b/ Evolution of the relative proportion of *OAl$_x$ sites as a function of milling time, as determined by quantifying the relative intensity of the *OAl$_x$ signal to that of the natural-abundance zirconia rotor peak (spectra shown in a/), and normalizing for the mass of sample introduced in the rotor (see supporting information, Figure S9). c/ ^{17}O MAS NMR spectrum recorded at 35.2 T for an Al_2O_3 phase enriched in ^{17}O by LAG, after 15 minutes grinding, followed by drying the sample at room temperature (this spectrum was recorded using a much shorter recycle delay and different excitation scheme than the one in Figure 3a); d/ ^{17}O MQMAS NMR spectrum recorded at 35.2 T, in which the *OAl$_x$ (dashed green circle) and Al$_x$*OH sites (dashed brown circle) are resolved. Colored bars above the spectra in Figures 3c and 3d correspond to the shift ranges expected for different oxygen environments, based on the literature.[12, 25-26, 31-32] Acquisition conditions can be found in supporting information (Table S1). "*" symbols correspond to spinning sidebands.

The different types of protons present around the enriched oxygen sites were studied using fast MAS ^{1}H{^{17}O} HMQC (Heteronuclear Multiple Quantum Coherence) experiments at high magnetic field (20.0 T), looking at through-bond connectivities (J-HMQC), as well as through-space proximities

(D-HMQC). The main crosspeak observed on the 2D J-HMQC spectrum correlates the low frequency ^{17}O resonance (Al_x-*OH) to a ^{1}H resonance centered at ~ 3.8 ppm (Figure 4a). This ^{1}H chemical shift is consistent with a surface OH group acting as hydrogen-bond donor (denoted here μ-OH_{HBD}).[34] The significant linewidth of the ^{1}H resonance points to a distribution in μ-OH_{HBD}…O bond distances and angles.[34-35] Complementary 2D D-HMQC experiments were carried out to further characterize these hydroxyl environments (Figure 4b). At short recoupling time (τ_{rec} = 100 μs), the D-HMQC spectrum provides similar conclusions as the J-HMQC experiment, given that only correlations to the closest H atoms appear in these conditions, *i.e.* with hydrogen atoms which are directly bound to ^{17}O. In contrast, at longer recoupling times (τ_{rec} = 300 μs), an additional correlation is observed with *OAl_x resonances. This points to the close proximity of some of the μ-OH_{HBD} protons to *OAl_x sites, possibly due to μ-OH_{HBD}…*OAl_x hydrogen bonds. It is worth noting that recent computational studies of γ-alumina surfaces suggest that μ-OH_{HBD}…OAl_x hydrogen bonds can indeed be present at the surface.[34] The diversity of H-bonding environments of surface hydroxyls can thus account, at least in part, for the distribution in oxygen environments around the Al_x-*OH and *OAl_x moieties mentioned above (Figure 3d).

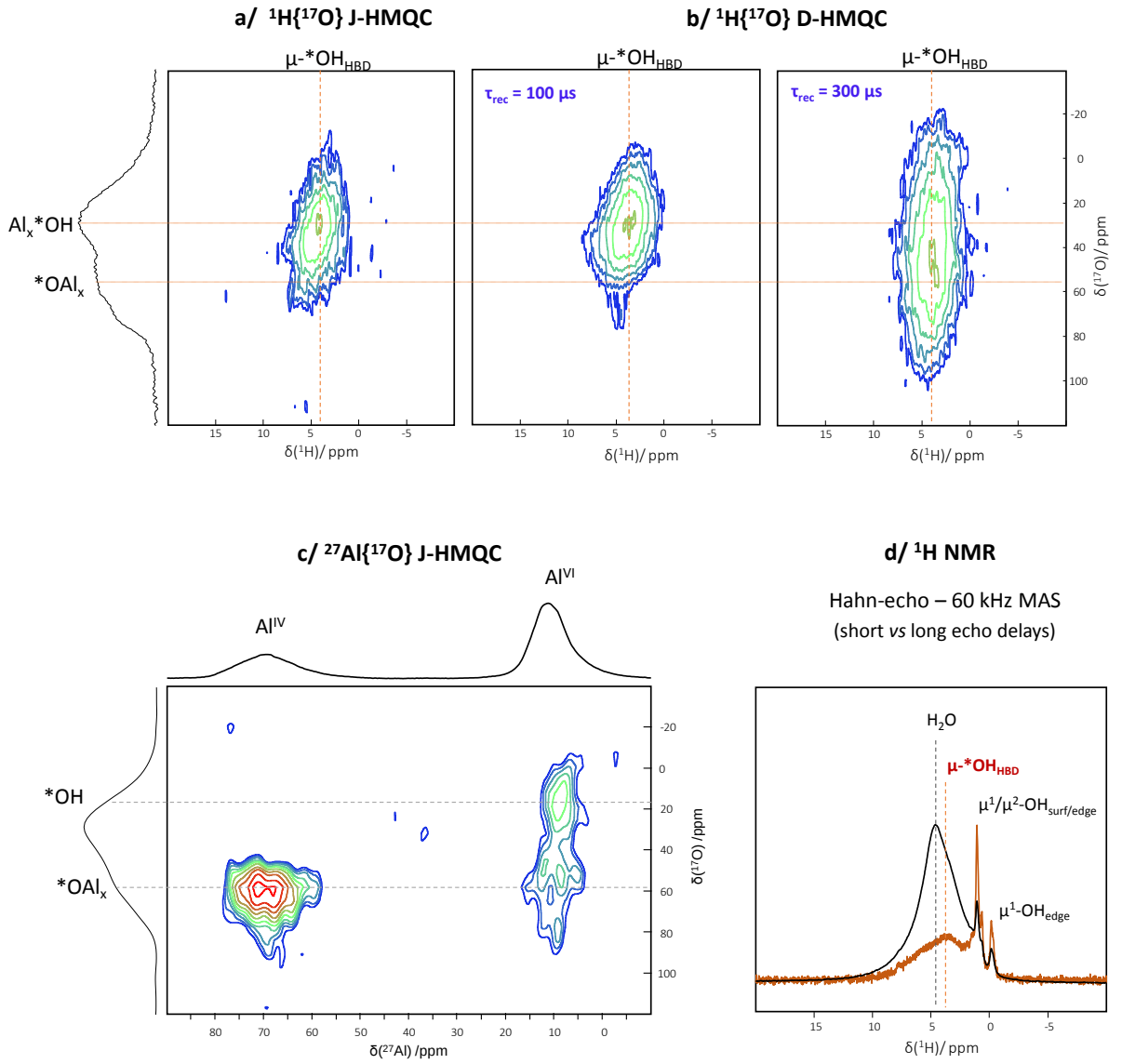

Figure 4. a/^{1}H{^{17}O} J-HMQC NMR spectrum recorded at 20.0 T and 60 kHz MAS on an Al_2O_3 phase enriched in ^{17}O by LAG after 15 minutes grinding, followed by drying the sample at room temperature; the projection corresponds to the DFS-1pulse signal for this phase; b/ ^{1}H{^{17}O} D-HMQC NMR spectra recorded at 20.0 T and 60 kHz MAS on the same phase, using 2 different recoupling times (100 and 300 μs); c/ ^{27}Al{^{17}O} J-HMQC spectrum recorded at 20.0 T for an Al_2O_3 phase enriched in ^{17}O by LAG (15 min BM), after drying under vacuum at room temperature (the total acquisition time was ~50 h for this spectrum). Projections correspond to Hahn-echo spectra recorded for the sample at this magnetic field; d/ ^{1}H Hahn echo NMR spectra recorded at 20.0 T and 60 kHz MAS, using echo delays of 2 (black) and 50 (brown) rotor periods (see Figure S10 in Supporting Information for comparison to the background ^{1}H NMR spectrum). ^{1}H resonances are assigned based on recent literature (HBD = hydrogen bond donor).[34]

To go one step further, a ^{27}Al{^{17}O} J-HMQC experiment was performed, to see which of the hexacoordinate (Al^{VI}) and tetracoordinate (Al^{IV}) sites of alumina were linked to *OAl_x and Al_x-*OH moieties (Figure 4c). Three crosspeaks are observed on the 2D spectrum, which provide direct evidence of the presence of Al^{VI}- *OH, Al^{VI}-*O and Al^{IV}-*O bonds. Considering the *OAl_x sites, this spectrum clearly shows that part of the chemical shift distribution observed in Figure 3d can come not

only from the number but also from the type of aluminum atoms attached to the oxygen (Al^{IV} and/or Al^{VI}).

The lack of Al^{IV}-*OH correlations in Figure 4c may seem surprising when considering the ^{1}H MAS NMR data (see Figures 4d and S10). Indeed, the 1D ^{1}H NMR spectrum (which was recorded using two different echo delays to achieve better resolution) shows sharp resonances, notably at ~ –0.2, 0.7 and 1.1 ppm. Based on the literature, these could correspond to terminal (μ^1-OH) and bridging (μ^2-OH) sites,[34, 36] located at the surfaces and edges of alumina particles. In particular, the signal at –0.2 ppm has recently been attributed to μ^1–OH species present at the edges,[34] which are likely to be linked to tetrahedral Al^{IV} sites.[36] This would imply that while Al^{IV}-OH species appear to be present in the sample, they could not be detected in ^{17}O NMR. Several explanations can be proposed to this. First, this observation could be consistent with the known difference in reactivity of the different surface hydroxyls.[34, 37] Indeed, it is possible that upon exposure of the sample to air and hence ambient humidity (when recovering the sample after the LAG step or during the packing/unpacking of NMR rotors), some of the enriched Al-*OH groups back exchange with non-labeled hydroxyls. The fact that the samples are still porous after LAG would indeed be in favor of surface exchanges of reactive OH groups, which would be more likely to occur for the hydroxyls which are more reactive and/or less tightly bound, as would be the case for μ^1-OH and μ^2-OH groups with ^{1}H resonances below 3 ppm, which are not involved in strong H-bonds.[34] This exchange would also be consistent with the fact that on the $^{1}H\{^{17}O\}$ J-HMQC data, only the ^{1}H resonances of the hydrogen-bonded μ-OH groups at ~ 3.8 ppm correlate to the Al_x-*OH resonance, but not those at ~ –0.2, 0.7 and 1.1 ppm (due to their back-exchange). Second, from a purely NMR perspective, it is also possible that the small proportion of μ^1-OH and μ^2-OH resonances (shown by ^{1}H NMR), combined to a potentially smaller values of J couplings, renders them "invisible" in the $^{27}Al\{^{17}O\}$ 2D experiment (Figure 4c). All the above reasons could explain (at least in part), why no cross-peak correlating Al^{IV} sites to OH groups could be observed on the $^{27}Al\{^{17}O\}$ J-HMQC spectrum.

The observation of the progressive formation of $*OAl_x$ sites (Figure 3b), and the potential back-exchange of some of the enriched hydroxyls, prompted us to use ^{17}O DNP SENS (surface enhanced NMR spectroscopy)[38-39] to examine the nature of the oxygen environments present at the *surface* of the alumina particles. DNP analyses were performed on a sample recovered after 15 minutes milling, after impregnation by a biradical solution of TEKPol in deuterated tetrachloroethane. Two types of NMR sequences were used, as a means to polarize differently the surface atoms oxygen during microwave irradiation: *(i)* direct-excitation ^{17}O NMR (preceded by a double-frequency sweep enhancement), in order to polarize the surface oxygen sites directly from the radical, and *(ii)* $^{17}O\{^{1}H\}$ CPMAS, where ^{17}O sites are detected based on their relative proximity to the protons polarized by the biradical (by varying the contact time used). In both situations, the ^{17}O NMR signals of $*OAl_x$ and *OH groups were found to be enhanced upon microwave irradiation (Figure 5), suggesting that both of these ^{17}O environments are present at the surface of the alumina particles. In particular, under $^{17}O\{^{1}H\}$

DNP CPMAS conditions (Figure 5), both sites were enhanced by a factor ~ 4, meaning that protons located at the surface of the particles after LAG can transfer their polarization to neighboring Al-*OH (at short contact time) and *OAl$_x$ sites (at longer contact time). Although these DNP-SENS experiments did not allow any absolute quantification of the relative labeling of the bulk or surface of the material, they clearly suggest that some enriched oxygen sites are still present at the surface of the particles, despite possible partial $^{17}O/^{16}O$ back-exchanges upon exposure of the sample to ambient atmosphere.

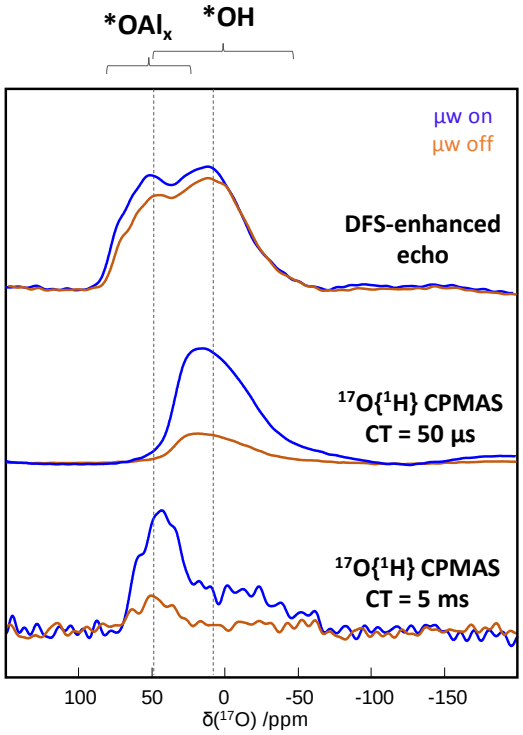

Figure 5. ^{17}O DNP experiments carried out at 14.1T on an Al_2O_3 phase enriched in ^{17}O by 15 minutes LAG (followed by drying the sample at room temperature), and impregnation by TEKPol/D_2-TCE: *(i)* Direct-excitation ^{17}O DNP NMR spectra (with a DFS enhancement), and *(ii)* $^{1}H\{^{17}O\}$ CPMAS DNP NMR spectra recorded at 50 µs and 5 ms contact times (CT). Spectra recorded without (brown) and with (blue) microwave irradiation are compared (µw on / µw off). DNP acquisition conditions and enhancements are discussed in Supporting Information (S11), and comparisons to ^{17}O NMR data recorded at room temperature are reported in Figure S12.

In summary, although the overall structure of alumina appears to be maintained during the LAG step (according to X-ray diffraction and ^{27}Al NMR), part of this phase actually undergoes several reactions in the presence of H_2*O, leading to a change in texture of the material, and to the formation of Al$_x$-*OH and *OAl$_x$ species. The fact that *OAl$_x$ environments were detected after only 5 minutes of milling underscores that the condensation of Al$_x$-*OH groups proceeds very quickly under the reaction conditions used here. For both Al$_x$-*OH and *OAl$_x$ species, high resolution NMR experiments were able to shed light on the diversity of oxygen local environments, due to the presence of hydrogen bonds and differences in the nature and number of Al-sites to which they are bound.

Moreover, ^{17}O DNP-SENS experiments were performed, suggesting that some of the enriched Al_x-*OH and *OAl_x sites are located at the surface of the particles.

Titania

Enriched titania phases were studied by ^{17}O MAS NMR after different LAG times (1 min, 15 min and 1 hour). NMR spectra were recorded both on "fresh" samples, which were analyzed by NMR directly after milling, and on samples which had undergone an additional drying step at room temperature. In all cases, signals belonging to *OTi_3 environments were observed around 550 ppm. The resonance characteristic of crystalline anatase was found to increase with the milling time (signal at 560 ppm, Figure 6a). Weaker underlying resonances, which span between 500 and 600 ppm (Figure 6b), were also observed at all milling times, and can be ascribed to more distorted/disordered *OTi_3 environments and surface defects.[9, 28, 40]

In the case of the "fresh" phases, residual ^{17}O labeled water was detected at ~0 ppm. Its relative proportion was found to decrease as the milling time increased (Figure 6a). However, no clear evidence of Ti-*OH groups was observed. Based on the literature, Ti-*OH resonances were expected to be centered just above 200 ppm.[9, 40-41] Complementary ^{17}O DNP SENS analyses were thus carried out to try to detect more clearly the surface species (Figures 6c-d), and bring direct evidence of Ti-*OH groups (if any). First, it is worth noting that at low temperatures such as those used for DNP analyses (~100 K), a very weak signal could be detected at ~200 ppm, suggesting the presence of a small number of Ti-*OH species. Dynamics within the Ti-*OH moieties at room temperature may explain why they could not be detected by conventional NMR. This signal could then be enhanced by direct excitation ^{17}O-DNP (Figure 6c), and even more so using DNP $^{17}O\{^1H\}$ CPMAS experiments at very short contact times (Figure 6d). Indeed, the main signal observed by DNP $^{17}O\{^1H\}$ CPMAS for 50 μs contact time was centered at ~200 ppm.

Based on previous experimental and computational studies reported in the literature, the extent of water dissociation on anatase surfaces is known to be highly dependent on several parameters, including the nature of the surface exposed and the extent of surface defects.[42-43] Hence, it is possible that the formation of Ti-*OH groups by dissociation of H_2*O on anatase requires the creation of reactive surfaces by mechanochemistry. Moreover, given that very few Ti-*OH species could be detected at the surface of the materials (even for "fresh" phases), it is possible that these recondense quickly to form *OTi_x sites under the reaction conditions used here. Overall, this would explain the evolution of the reaction medium shown in Figure 6a.

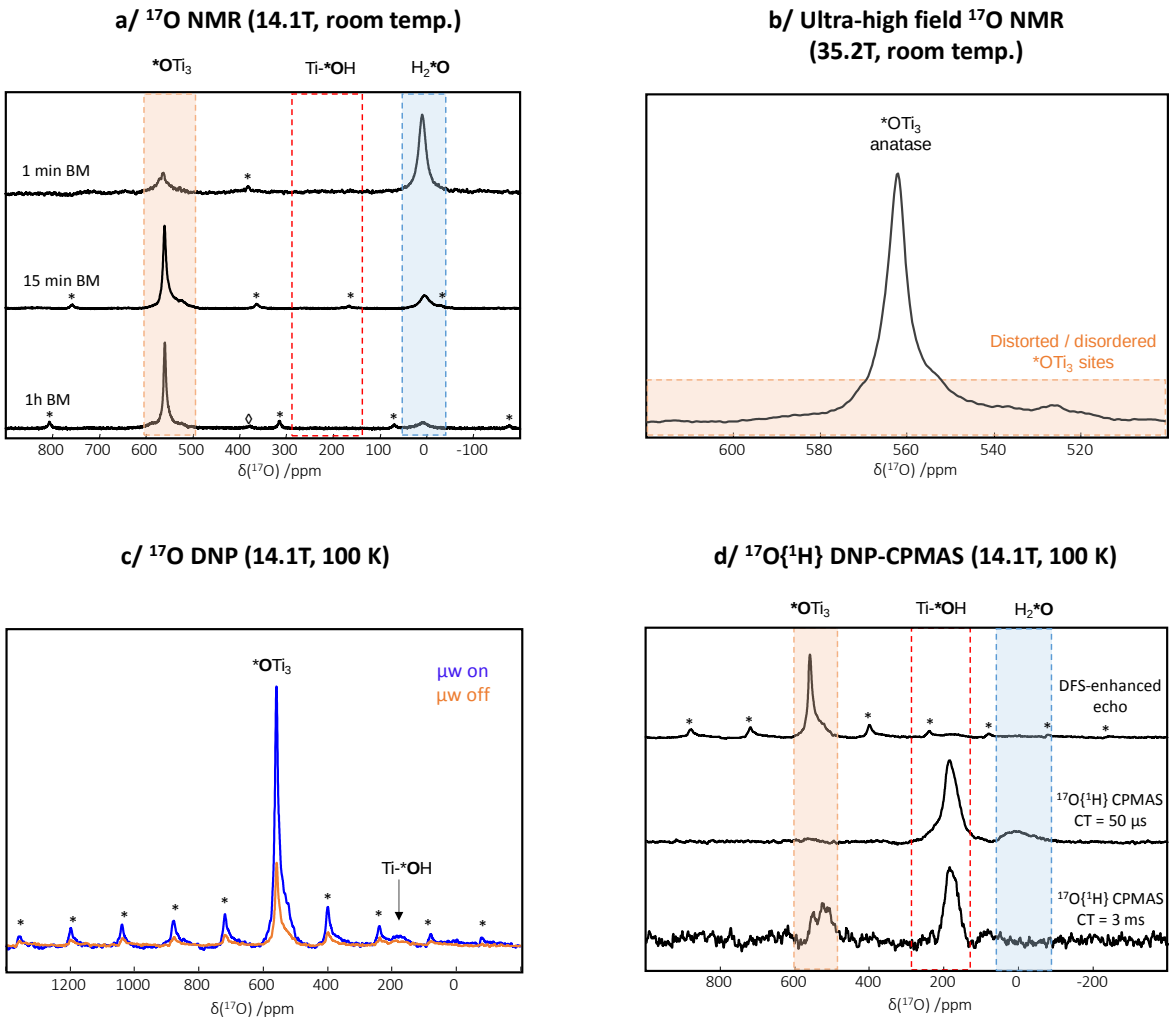

Figure 6. a/ ^{17}O MAS NMR spectra recorded at 14.1T on "fresh" TiO_2 phases enriched in ^{17}O by LAG (for 1 min, 15 min and 1 hour milling times); b/ ^{17}O MAS NMR spectrum recorded at 35.2T on a TiO_2 phase enriched in ^{17}O by LAG (15 min BM), after drying under vacuum at room temperature; c/ ^{17}O DNP NMR spectrum of a TiO_2 phase enriched in ^{17}O by LAG (15 min BM), after drying under vacuum at room temperature, and impregnation by a 16 mM solution of TEKPol in TBE (spectra recorded at ~100 K, with and without microwave irradiation); d/ ^{17}O{^{1}H} DNP-CPMAS spectra recorded at 50 µs and 3 ms contact times, in comparison to the DFS-enhanced echo spectrum recorded at ~100K. All acquisition parameters can be found in Table S1 (supporting information). * symbols correspond to spinning sidebands, and ◊ symbols to the zirconia rotor background signal.

DNP SENS analyses were able to provide additional information regarding the other enriched oxygen sites which were present close to the surface, aside from the Ti-*OH moieties. First, when analyzing the results of the DNP experiments performed with direct ^{17}O acquisition (Figure 6c), it is clear that bulk-like *OTi_3 environments are also present close to the surface of the particles. Second, by increasing the contact time in the DNP ^{17}O{^{1}H} CPMAS experiment, it was possible to observe weak resonances in the *OTi_3 region (Figure 6d, CT = 3 ms). These correspond to oxygen species which are spatially close to protons (but not directly bound to them) and appear to contribute to the "underlying" disordered/distorted Ti*O_3 resonances detected in Figure 6b. Such detailed information

on the different oxygen environments is expected to be of high interest for proposing realistic models of the anatase surface recovered after the milling step, by combining computational modeling to *ab-initio* calculations of ^{17}O NMR parameters, and comparing results to experimental ^{17}O NMR data, as previously proposed for other studies on titania surfaces.[9, 44]

To sum up, although the overall structure of anatase appears to be maintained according to X-ray diffraction, the texture of the material is affected by the milling process, and ^{17}O NMR further shows that this phase reacts with labeled water to form enriched anatase-like *OTi_3 environments after only 1 minute of milling. However, in contrast to alumina, only a very small number of labeled *OH species were observed in the 1D ^{17}O MAS NMR spectra (even when analyzing freshly recovered samples), and these could only be clearly detected using DNP-SENS analyses.

Silica and zirconia

Preliminary investigations were also performed at different milling times on silica and zirconia. For the former (Figure 7a), characterizations after only 1 minute milling suggested the presence of both silanols (Si-*OH) and siloxanes (Si-*O-Si). The significant proportion of siloxane bridges after 1 minute of milling is particularly noteworthy, because it demonstrates that the condensation reactions of intermediate Si-*OH groups proceeds quickly under the reaction conditions used here. In contrast, in the case of zirconia, it was found that the ^{17}O-enrichment using LAG is much more challenging to achieve. Indeed, the two resonances characteristic of the monoclinic form were barely visible after 15 minutes milling (Figure 7b). Moreover, no direct evidence of Zr-*OH groups could be detected by conventional ^{17}O NMR (these being expected around ~ 100 ppm).[10] The underlying resonances observed as a shoulder around 400 ppm after 1 hour of milling may be due to more disordered *OZr_x environments. Further investigations are currently in progress on these phases, both from the synthesis and NMR/DNP points of view, in order to better characterize and control the nature of enriched *OM_x and M-*OH groups at different milling times, and to establish the optimal conditions for isotopic labeling.

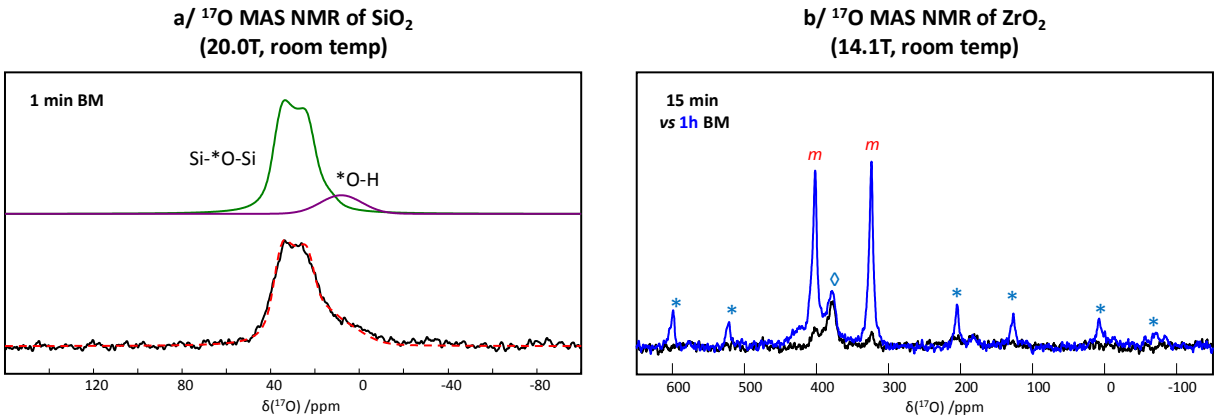

Figure 7. a/ ^{17}O MAS NMR analysis performed at 20.0T and 60 kHz MAS on a SiO_2 phase enriched in ^{17}O by LAG (1 min BM), after drying under vacuum at room temperature. The fit (dashed red line) was performed considering siloxanes (green) and silanols (purple). The silanol resonances could be more clearly resolved using $^{17}O\{^1H\}$ CPMAS analyses at short contact times (see Supporting Information, Figure S13), and their NMR signature is consistent with previous reports.[24, 45] b/ ^{17}O MAS NMR analyses performed at 14.1T and 20 kHz MAS on a ZrO_2 phase enriched in ^{17}O by LAG, after 15 min (black) and 1h (blue) milling. The "m" symbols indicate the two main resonances of monoclinic zirconia. * symbols correspond to spinning sidebands, and the ◊ symbol to the zirconia rotor background signal (see Figure S6).

3/ ^{17}O-labeling of mixtures of oxides: from liquid to solid oxygen-transfer reactions

Having demonstrated that it is possible to perform the direct ^{17}O-enrichment of simple oxides using LAG, the obvious next step was to see how mechanochemistry can be used to synthesize ^{17}O-labeled *mixed* oxides. Two mechanochemical approaches were considered to introduce the ^{17}O-label (Figure 8a): *(i)* milling the non-labeled oxide precursors together with H_2*O, or *(ii)* pre-enriching separately oxide precursors, before 'dry'-milling them together. While the former strategy was recently used for enriching the lithium-ion battery electrode materials like Li_2RuO_3,[7] no ^{17}O NMR analysis of the milling medium just after the LAG step was reported. Moreover, comparing the two strategies may actually shed light on how oxides react with each other in the solid state during mechanochemical reactions.

These two approaches were tested on a TiO_2/SiO_2 mixture, using the same oxide sources as mentioned previously (mesoporous anatase and amorphous silica), with the aim of comparing the media recovered just after the milling step, *i.e.* before any further heat treatment. On one hand, equimolar quantities of TiO_2 and SiO_2 were milled together by LAG using H_2*O. On the other hand, a pre-enriched Ti*O_2 phase was dry-milled in presence of an equimolar quantity of non-labeled SiO_2. Both media were compared after 3 minutes BM. Although the XRD patterns were found to be the same (Figure 8b), their solid-state NMR spectra were completely different (Figure 8c).

In the LAG case, the ^{17}O signatures of enriched titania and silica were both visible, but with a significant discrepancy in their relative enrichment, the vast majority of the isotopic label having entered the silica phase (Figure 8c, black curve). Interestingly, in addition to the *OTi_3 and siloxane resonances, it is worth noting that a broad signal is also observed between ~ 450 and 100 ppm, i.e. in a zone which covers the range expected for *OTi_4, Si-*O-Ti and Ti-*OH groups.[46-47] The more distinct

contribution around ~200 ppm could be indicative of the formation of a small number of Ti-*OH groups under these synthetic conditions.

In the Ti^*O_2/SiO_2 "dry-milling" case, although the $^*OTi_3$ anatase signal is still predominant, a broad signal is also detected between ~ 450 and 100 ppm, as well as a new resonance around ~30 ppm (Figure 8c, red curve). The latter resonance can be assigned to enriched Si-*O-Si bridges (see Figure S14 in supporting information, for an expansion into the siloxane region). Given that the silica precursor was initially non-labeled, this clearly points to the fact that the reactions occurring at the interface of Ti^*O_2 and SiO_2 during the ball-milling eventually result in bonding rearrangements around the oxygen atoms, which lead to the enrichment of the silica phase. More importantly, such an "oxygen transfer" between the two oxides starts to occur after just 3 minutes, meaning that very short milling times are sufficient to mix the reagents intimately, so that they can start reacting at their interface.

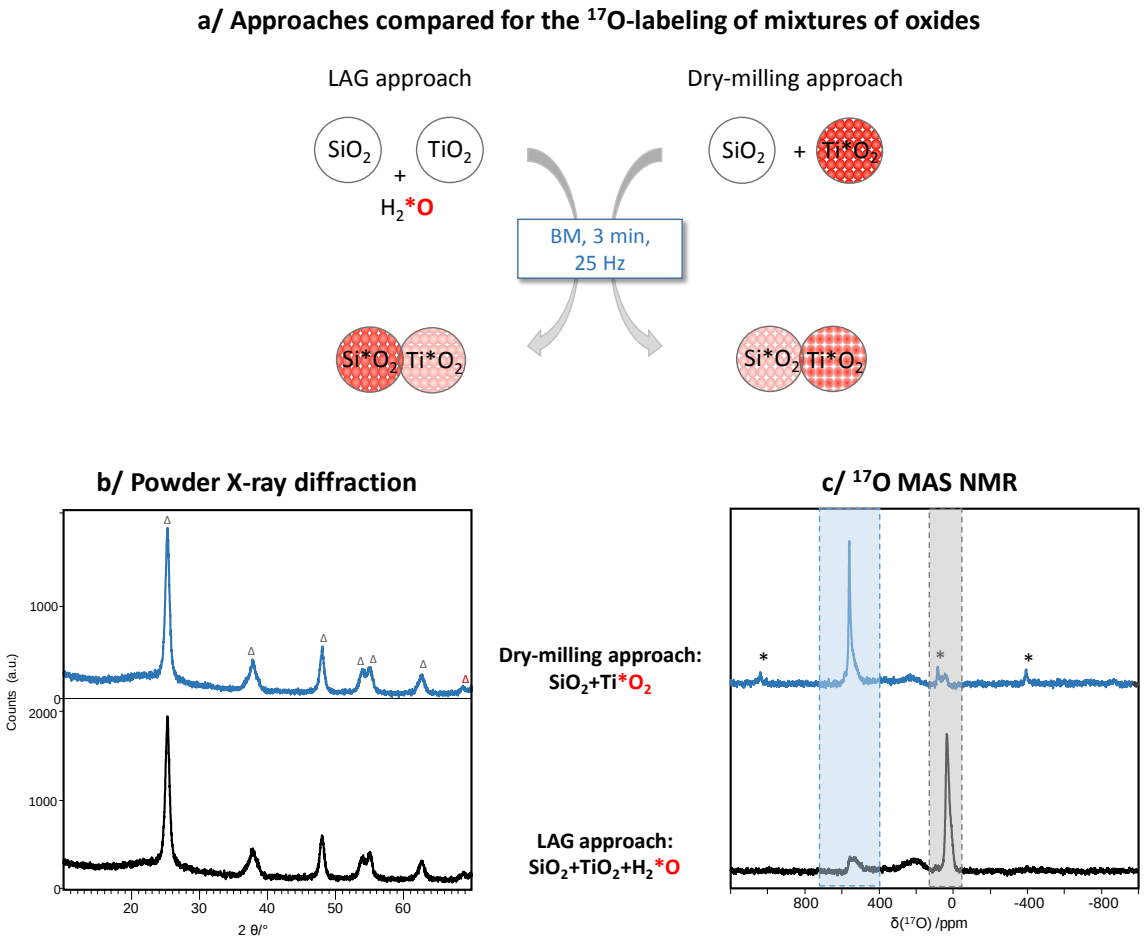

Figure 8. a/ Schematic representation of the two synthetic approaches tested for enriching mixtures of SiO_2 and TiO_2 in ^{17}O using mechanochemistry (shades of red are used to reflect the average relative ^{17}O-labeling of the oxides after milling); **b/** and **c/** Characterizations of ^{17}O-enriched SiO_2/TiO_2 mixtures using PXRD and ^{17}O MAS solid state NMR at 20T. *Top:* Dry-milling of non-labeled SiO_2 with enriched Ti^*O_2 for 3 minutes (blue curves). *Bottom:* LAG of a mixture of TiO_2 and SiO_2 for 3 minutes in presence of $H_2{}^*O$ (black curves). "Δ" symbols correspond to the diffraction peaks of anatase in PXRD (ICSD #7206075), and "*" symbols correspond to spinning sidebands in ^{17}O NMR. The shaded regions on the ^{17}O MAS NMR

spectra correspond to the chemical shifts expected for OTi_x (light blue) and siloxane (light grey) environments. An expansion of the ^{17}O NMR spectra in the siloxane region can be found in Figure S14.

The comparison of the two ^{17}O-labeling approaches points to the major advantages of ^{17}O NMR for studying the reactivity of inorganic oxides in BM and helps understand better the differences in reactivity of oxides during ball-milling. On one hand, it allows identifying the different oxygen environments present, thereby revealing oxygen bonding rearrangements which occur at the interfaces between the oxides. On the other hand, it can also bring clear evidence of discrepancies in oxygen isotopic distribution within samples. Moreover, the $H_2{}^{17}O$-LAG approach used here could more generally help shed light on differences in reactivity of liquid grinding assistants like water with respect to the different components of a mixture, a feature which has not been looked into so far.

4/ Discussion

New ^{17}O-enrichment approaches for oxides

The enrichment strategies described above significantly broaden the scope of approaches available for producing ^{17}O-enriched s-, p- and d- block oxides, and offer synthetic alternatives which are highly efficient, both in terms of cost and practicality. One of the reasons to this comes from the nature of the precursors involved: oxides and ^{17}O-enriched water. Oxides are indeed very interesting starting materials because they are either directly commercially available (as for TiO_2, SiO_2, Al_2O_3 and ZrO_2), or because they can be easily produced by heat treatment of hydroxides (as illustrated here for CaO and Li_2O) or even carbonates. Moreover, being able to perform the ^{17}O-labeling on commercially available sources of titania, silica, alumina and zirconia, which can be stored and handled under ambient conditions for several months, is a key advantage in comparison to other procedures used so far for enriching these phases, in which more sensitive alkoxide or chloride precursors had been used.[12-15, 46, 48-51] Indeed, no safety hazard was involved here in the LAG step, which could be easily scaled up to produce gram quantities of labeled material, which contrasts with syntheses involving highly reactive and toxic reagents such as $SiCl_4$ and $TiCl_4$. Although the maximum ^{17}O-enrichment is meant to be higher in the latter case (as the only source of oxygen is ^{17}O-enriched water), the ^{17}O content of the phases recovered after LAG was nevertheless sufficient for performing a wide range of high-resolution NMR experiments, as shown in the case of the 2D ^{1}H-^{17}O and ^{27}Al-^{17}O MAS NMR experiments performed on alumina (Figures 4a-c). Moreover, it is expected that further optimizations of the LAG step could lead to higher enrichments than those achieved so far, by increasing the amount of H_2*O added, varying the texture/porosity of the oxide precursor used, and/or optimizing the ball-milling conditions. Indeed, a preliminary investigation on the ^{17}O-labeling of monoclinic zirconia phases of different initial crystallinity was performed, showing the importance of the choice of the precursor on the efficiency of the isotopic enrichment (see Supporting Information, Figure S15).

Using stoichiometric amounts of ^{17}O-enriched water for the labeling-step is also much less hazardous and constraining than having to manipulate ^{17}O-enriched O_2 gas at high temperatures, as

had been described in previous ^{17}O-enrichment protocols for oxides.[9-10, 12,52] Indeed, the labeling reactions were performed here under ambient temperature and pressure, and proceeded extremely quickly (less than 1 hour of milling). Moreover, in terms of cost, all syntheses were relatively cheap, amounting to less than ~ 40 euros for enriching ~ 50 mg of compound (when using 90% ^{17}O-enriched water in the syntheses). Overall, this implies that these protocols are expected to be accessible to both research and teaching laboratories, and to contribute to the development of advanced spectroscopic studies on various oxides (or oxide mixtures), which would require oxygen-17 (or oxygen-18) labeling.

Another very attractive feature of the protocols developed here is that the ^{17}O-enriched phases recovered after LAG can be used in multiple ways. First, they can be converted into related oxide phases by performing additional heat-treatments under inert conditions, as illustrated in Figure S16 for alumina and titania. Alternatively, they can directly serve as precursors for the synthesis of more complex mixed metal oxides, as illustrated in the previous section for the dry milling of Ti*O_2 with SiO_2. Last but not least, given that one of the unique properties of the enriched p- and d- block oxides produced here is that they are still mesoporous after LAG, with some of the surface sites enriched in ^{17}O (as suggested by DNP), they could be used as model systems for studying the surface reactivity of oxides by high-resolution ^{17}O NMR. In particular, considering the wide range of applications of transitional aluminas like γ- and δ- Al_2O_3 in heterogeneous catalysis, the ^{17}O-labeled alumina phases prepared by LAG could be of high interest to gain new insight into the surface reactivity of catalytic materials using high-resolution ^{17}O NMR and DNP.

Atomic-level insight into reactions occurring during ball-milling

Beyond the production of ^{17}O-enriched materials, our results also show how high-resolution ^{17}O NMR and DNP can help gain atomic-level information into LAG processes, and more generally reaction mechanisms in ball-milling. Mechanochemical reactions are indeed far from trivial, as they involve both physical steps (mixing of reagents, particle size reduction, creation of reactive surfaces, diffusion of atoms/molecules at the interfaces…) and chemical steps (chemical reactions), both of which are important for the system to evolve towards a given product.[53-54] Despite numerous investigations, some of which include *in situ* measurements and/or innovative designs of the milling equipment,[54-59] many blind spots remain regarding both the physics and chemistry of mechanochemical reactions. This is even more true when common techniques like X-ray diffraction are not informative, as observed here for the four p- and d- block oxides, as well as for the mixed SiO_2/TiO_2 system.

In the case of titania, alumina, and silica, ^{17}O NMR and DNP measurements at different milling times were able to provide clear evidence of the presence of intermediate M-*OH species, which can then condense to form *OM_x sites. One important point arising from these analyses was that the quantity of M-*OH sites detected differed significantly from one oxide to the other. In particular,

at the shortest milling times, while Al-*OH and Si-*OH groups could be clearly observed, this was not the case for Ti-*OH species, for which DNP analyses were needed to bring evidence of their presence. Given that several parameters can influence the formation of M-*OH groups (initial degree of covalency or ionicity of the M-O bonds within the oxide, texture and surface area of the material, and reactivity under the ball-milling conditions used), further investigations will be needed to determine the mechanism(s) by which enriched M-*OH groups form for each phase, *i.e.* whether it is by surface hydrolysis, dissociative adsorption of water, or exchange of labile M-OH groups initially present at the surface. From a more practical perspective, the differences in reactivity shown here demonstrate that milling conditions need to be optimized case by case for each oxide, in order to find how to achieve the highest ^{17}O-enrichment possible.

Based on the different high-resolution NMR experiments and the changes in porosity observed by N_2 volumetric analyses, it is reasonable to say that the initial formation of bulk-like *OM_x environments by ball-milling under ambient conditions results from the condensation of (transient) M-*OH sites. Due to these surface-reconstruction processes, which lead to changes in some of the oxygen-bonds of the initial particles, some enriched oxygen sites which were located at the surface of the oxide particles may become more "core-like". Under a given set of milling conditions, the extent of formation of these *OM_x sites and the depth of enrichment of the initial oxide particles depends on the nature and texture of the initial oxide, and the capacity of mechanochemistry to create "fresh" reactive surfaces to trigger these reactions.[53] This is illustrated when comparing the ^{17}O MAS NMR data and SIMS analyses of SiO_2 and TiO_2, and even more so when considering the different ^{17}O NMR analyses of Al_2O_3, as detailed below.

Concerning alumina, solid state NMR analyses also enabled to shed light on additional features of ball-milling reactions. First, as shown in Figure 3b, it is interesting to note that no "induction time" in the formation of *OAl_x species could be detected within the time scale investigated. Induction periods in ball-milling are generally made evident using X-ray diffraction techniques,[60-62] but such analyses would have led to an erroneous conclusion here, given that no change was observed in PXRD. Moreover, it is interesting to note that while an increase in the relative number of *OAl_x environments with time was observed, it progressively slowed down after the first 15 minutes. Given that Al-*OH and *OAl_x environments very easily formed during the milling (as they were detected after only 5 minutes of reaction), this suggests that other rate-limiting steps takeover after 15 minutes. It is possible that the enrichment of *OAl_x sites then proceeds by other mechanisms, involving the gradual rearrangement of oxygen bonding environments within the intermediate oxy-hydroxy phase. Alternatively, changes in the texture and rheological properties of the medium (due to the progressive consumption of enriched water and/or modification of the mesoporosity of the material) may render the milling process less efficient in creating new reactive surfaces, thereby slowing down the speed of enrichment. To go one step further, additional high-resolution ^{17}O NMR and DNP analyses will be needed to study the relative binding of oxygen atoms to

Al^{IV} and Al^{VI} sites as a function of milling time, and the reactivity of the different surface *OH groups created by LAG. This should, in return, help rationalize the enrichment process at the atomic level, and better control the nature and proportion between the enriched sites.

Finally, the studies on the mixed SiO_2/TiO_2 system show how ^{17}O NMR can be used for looking at reactions occurring at the *interfaces* between different oxides during ball-milling. Indeed, the ^{17}O NMR characterization performed on the $\{SiO_2 + Ti^*O_2\}$ system demonstrate that after only 3 minutes of reaction, a variety of ^{17}O-enriched oxygen environments are present, which include enriched oxygen atoms within the silica phase. Being able to provide such atomic-level insight at the very early stages of the reaction is important to evaluate the efficiency of a given milling process to mix different solid particles (whether they are crystalline or amorphous, as is the case here), and to create contacts between them which will allow solid/solid reactions to occur. More generally, such analyses will certainly help understand better what *chemical* reactions occur during ball-milling when disordered or amorphous phases are involved, such reactions being intrinsically very complex to study.

Conclusion

In this manuscript, we have shown how the ^{17}O-labeling of oxides using mechanochemistry can be used for two main purposes: *(i)* preparing ^{17}O-enriched oxides, and *(ii)* understanding reaction mechanisms occurring during ball-milling. Concerning the first point, liquid assisted grinding in presence of ^{17}O-enriched water was shown to be a highly attractive enrichment strategy for the fast and straightforward labeling of simple oxides of the s, p and d blocks, starting from the non-labeled oxide precursors. Regarding the second point, it was demonstrated how thanks to mechanochemistry-mediated isotopic labeling, it becomes possible to address questions regarding the physical and chemical processes occurring at the atomic level during ball-milling, by performing advanced ^{17}O solid state NMR analyses, including ultra-high-field NMR, DNP and fast-MAS measurements. In this context, one of the highlights of this work is to shed light on what chemical reactions start occurring at the interfaces between different oxide particles in the first few minutes of milling. Given that milling together inorganic precursors is frequently one of the first steps in the synthesis of functional mixed-metal oxides, performing similar high-resolution ^{17}O NMR analyses on different mixtures of enriched oxide precursors and under different milling conditions could not only help optimize the milling process, but also help identify intermediate phases, which could in turn serve for the preparation of novel materials.

Experimental section

Synthesis of ^{17}O-labeled phases

Reagents and milling equipment. Calcium hydroxide ($Ca(OH)_2$, Sigma-Aldrich, ≥ 96%) and lithium hydroxide monohydrate ($LiOH.H_2O$, Prolabo Normapur, Analytical Reagent, ≥ 99.0%) were used as received, and served as precursors for the synthesis of CaO and Li_2O. Silica (SiO_2, Aerosil 200, Degussa, 180 m^2/g), alumina (Al_2O_3, "aluminoxid C", Degussa, mixture of γ- and δ- forms, 100 m^2/g), titania (TiO_2, St-Gobain Norpro, anatase phase, 150 m^2/g), and zirconia (ZrO_2, St-Gobain Norpro, monoclinic form, 85 m^2/g) were dried under vacuum for 3 to 4 hours at room temperature prior to use. ^{17}O-labeled water (with 40% or 90% ^{17}O-enrichment) was purchased from CortecNet. ^{18}O-labeled water (with 97% ^{18}O-enrichment) was purchased from Eurisotop. For DNP experiments, TEKPol[63] was purchased from Cortecnet.

All milling treatments were carried out at ~ 22°C (± 3 °C) in a Retsch Mixer Mill 400 apparatus, using 10 mL stainless steel grinding jars with screw top or push-fit lids. Unless otherwise noted, the protocols were first tested in triplicate using non-labeled water, before performing the experiments with ^{17}O (or ^{18}O) -enriched H_2O.

Synthesis of Ca(*OH)$_2$ and Ca*O. Non-labeled $Ca(OH)_2$ was first heat-treated to 950°C in a tubular furnace under Ar atmosphere (heating rate: 10°C / min; dwell-time at 950°C: 4 h) to produce CaO. The freshly prepared CaO phase (50 mg, 0.9 mmol, 1 eq) was introduced in the grinding jar together with 16µL of 40%-enriched $H_2{}^{17}O$ (0.9 mmol, 1 eq) with two stainless steel balls (10 mm diameter). The jar was closed and subjected to grinding for 1 hour in the mixer mill operated at 25Hz. The reactor was opened and the white powder, which progressively dries upon contact with air, was recovered by scraping the edges of the reactor and beads with a spatula, and characterized by XRD and ^{17}O solid state NMR, showing the formation of $Ca(*OH)_2$. (Average yield (n = 4): 54 mg, 82%). ^{17}O-enriched CaO was then synthesized by heat-treating the labeled hydroxide for 4 h at 950°C in a tubular furnace under Ar atmosphere, using the same conditions as above.

LAG of SiO$_2$. SiO_2 (50 mg, 0.84 mmol, 1.0 eq) was introduced in a screw top grinding jar with ^{17}O-labeled water (15 µL, 0.83 mmol, 1.0 eq) and two stainless steel balls (10 mm diameter). The jar was closed and subjected to grinding for milling times ranging from 1 minute to 1 hour, in the mixer mill operated at 25 Hz. The reactor was opened, and the sample was recovered by scraping the edges of the reactor and beads with a spatula (average mass of the crude material (n = 4): 60 mg). The recovered sample was white for short milling times, but light grey beyond 15 minutes milling (see supporting information, Figure S2, for EDXS analyses). Samples were then dried under vacuum at room temperature.

LAG of Al$_2$O$_3$. Al_2O_3 (50 mg, 0.49 mmol, 1.0 eq) was introduced in a grinding jar with ^{17}O-labeled water (13 µL, 0.72 mmol, 1.5 eq) and one stainless steel ball (10 mm diameter). The jar was closed and subjected to grinding for milling times ranging from 5 minutes to 1 hour in the mixer mill

operated at 25 Hz. The reactor was opened, and the solid powder was recovered by scraping the edges of the reactor and beads with a spatula (average mass of the crude material (n = 4): 45 mg). The recovered sample was white for short milling times, but very light grey beyond 15 minutes milling (see supporting information, Figure S3, for EDXS analyses). Depending on the sample, further treatments were performed, either under vacuum at room temperature, or at high temperature under Ar atmosphere (heating rate: 10°C / min; dwell-time at 900°C: 4 h – see Figure S16).

LAG of TiO_2. TiO_2 (50 mg, 0.63 mmol, 1.0 eq) was introduced in a grinding jar with ^{17}O-labeled water (11 μL, 0.61 mmol, 1.0 eq) and one stainless steel ball (10 mm diameter). The jar was closed and subjected to grinding for milling times ranging from 1 minute to 1 hour in the mixer mill operated at 25 Hz. The reactor was opened, and the solid powder was recovered by scraping the edges of the reactor and beads with a spatula (average mass of the crude material (n = 4): 44 mg). The recovered sample was white for short milling times, but light grey/yellowish beyond 15 minutes milling (see supporting information, Figure S4, for EDXS analyses). Depending on the sample, further treatments were performed, either under vacuum at room temperature, or at high temperature under Ar atmosphere (heating rate: 10°C / min; dwell-time at 900°C: 4 h – See figure S16).

LAG of ZrO_2. ZrO_2 (50 mg, 0.41 mmol, 1 eq) was introduced in a grinding jar with ^{17}O-labeled water (7 μL, 0.39 mmol, 1 eq) and one stainless steel ball (10 mm diameter). The jar was closed and subjected to grinding for milling times ranging from 15 minutes to 1 hour in the mixer mill operated at 25 Hz. The reactor was opened, and the solid powder was recovered by scraping the edges of the reactor and beads with a spatula (average mass of the crude material (n = 4): 42 mg). The recovered sample was white for short milling times, but very light grey beyond 15 minutes milling (see supporting information, Figure S5, for EDXS analyses). Samples were then dried under vacuum at room temperature.

LAG of TiO_2 and SiO_2. TiO_2 (28.3 mg, 0.35 mmol, 1 eq) and SiO_2 (21.5 mg, 0.35 mmol, 1 eq) were introduced in a grinding jar with ^{17}O-labeled water (13 μL, 0.72 mmol, 2 eq) and one stainless steel ball (10 mm diameter). The jar was closed and subjected to grinding for 3 minutes in the mixer mill operated at 25 Hz. The reactor was opened, and the white powder was recovered by scraping the edges of the reactor and beads (m ~ 43 mg).

BM of Ti^*O_2 with SiO_2. Ti^*O_2 was first synthesized as described above, by milling TiO_2 for 15 minutes, and then drying the sample under vacuum for 1 hour at room temperature. Then, labeled Ti^*O_2 (28.6 mg, ~0.35 mmol, 1 eq) was introduced in a grinding jar with non-labeled SiO_2 (21.4 mg, 0.35 mmol, 1 eq) and one stainless steel ball (10 mm diameter). The jar was closed and subjected to grinding for 3 minutes in the mixer mill operated at 25 Hz. The reactor was opened, and the solid powder was recovered by scraping the edges of the reactor and beads (m = 42 mg).

Characterization techniques

Powder X-ray diffraction. Powder XRD analyses were carried out on a Philips X'pert Pro MPD diffractometer using Cu Kα1 radiation (λ = 1.5406 Å) in Bragg-Brentano scanning mode with a 2θ angle between 10 and 70˚, and a time per step ranging from of 30 to 240 s, depending on the sample.

Scanning Electron Microscopy and EDXS analyses. SEM measurements were conducted on a Hitachi S4800 instrument under an excitation voltage between 0.5 and 8.0 kV depending on each powder's surface charging. For SEM, powdered samples were deposited on double sided conducting carbon tape and then Pt-metallized by sputtering under vacuum. EDXS analyses were carried out on a Zeiss Evo HD15 scanning electron microscope equipped with an Oxford Instruments X-MaxN SDD 50 mm^2 EDX detector. For EDXS, powdered samples were deposited on double sided conducting carbon tape and then metallized with carbon before analyses.

N_2 adsorption/desorption isotherms. N_2 volumetric analyses were performed by physisorption of N_2 using a Tristar instrument (Micromeritics, Norcross, USA). Prior to measurements, samples were degassed under vacuum overnight at 150 ˚C.

Surface Ion Mass Spectrometry (SIMS). SIMS analyses were performed on *(i)* SiO_2 and TiO_2 samples which had been enriched by LAG as described previously (1h BM), but using 97% ^{18}O-labeled water, and *(ii)* non-labeled SiO_2 and TiO_2 phases, which served as controls. All samples were pelletized, dried under vacuum, and then sputtered by a thin layer of gold prior to analysis. Measurements were performed on the IMS4F apparatus (Cameca) of the Geosciences Platform of the University of Montpellier, equipped with a 10 keV Cs sputter gun. For each sample, average $^{18}O/^{16}O$ ratios were determined by analyzing 3 different zones of the surface, and performing 5 blocks of 10 measurements on each zone.

^{17}O solid state NMR – 1D experiments. The majority of ^{17}O solid state NMR experiments were performed on a Varian VNMRS 600 MHz (14.1 T) NMR spectrometer, using either Varian 3.2 mm HX or HXY probes, or a Phoenix 3.2 mm probe, tuned to ^{1}H (599.82 MHz) and ^{17}O (81.31 MHz). Spectra were recorded under magic angle spinning (MAS) conditions, with spinning speeds ranging from 16 to 20 kHz, depending on the sample. Additional ^{17}O MAS NMR experiments were performed on a Bruker 850 MHz (20.0 T) NMR spectrometer, using Bruker 1.3 or 3.2 mm probes, tuned to ^{1}H (850.23 MHz) and ^{17}O (115.26 MHz). Finally, ultra-high magnetic field experiments were also performed on the 1.5 GHz (35.2 T) SCH-instrument in Tallahassee,[64] using a 3.2 mm single-channel MAS probe, spinning at 18 kHz. The acquisition parameters used for each sample can be found in Table S1. ^{17}O-enriched $Ca(*OH)_2$ was used to set up the DFS (double-frequency sweep) enhancement scheme[65] and $^{17}O\{^{1}H\}$ CPMAS experiments. ^{17}O chemical shifts were referenced externally to tap water at 0.0 ppm (or to D_2O at -2.7 ppm).

^{27}Al solid state NMR – 1D experiments. ^{27}Al solid state NMR experiments were performed on a Varian VNMRS 600 MHz (14.1 T) NMR spectrometer, using a Varian 3.2 mm HX probe, or a Phoenix 3.2 mm probe, tuned to ^{1}H (599.82 MHz) and ^{27}Al (156.29MHz). Samples were packed into

low-Al background zirconia rotors for these measurements. Single-pulse experiments were performed spinning at 18 kHz, using a ^{27}Al excitation pulse of 0.7 μs (π/18 tip angle), a recycle delay of 6s, and acquiring a total of 512 transients. ^{27}Al{^{1}H} CPMAS experiments were performed spinning at 18kHz, using a ^{1}H excitation pulse of 6 μs (π/2 tip angle), and a contact time of 0.5 ms. The recycle delay was set to 1s, and the number of scans acquired ranged from 8000 to 61700, depending on the sample. ^{27}Al chemical shifts were referenced externally to a 1 M aqueous solution of $Al(NO_3)_3$.

^{1}H solid state NMR – 1D experiments. Fast MAS ^{1}H solid state NMR spectra were recorded on a Bruker 850MHz (20.0 T) instrument, using a Bruker 1.3 mm probe spinning at 60 kHz. A Hahn echo sequence was used, with π/2 and π pulses of 2.05 and 4.1 μs, and a rotor-synchronized echo delay corresponding to 2 or 50 rotor periods (Figure 4d). ^{1}H chemical shifts were referenced to a dipeptide (Asp-Ala), used as a secondary reference, the low frequency signal being set to 1.1 ppm with respect to tetramethylsilane. Additional Hahn-echo ^{1}H NMR spectra were also recorded on a Varian VNMRS 600 MHz (14.1 T) NMR spectrometer using a Phoenix 1.2 mm MAS probe, in order to evaluate potential contributions of background ^{1}H signals from the rotor and caps (see Figure S10, supporting information).

^{27}Al{^{17}O} J-HMQC. A ^{27}Al{^{17}O} J-HMQC MAS NMR experiment was performed on a Bruker 850MHz (20.0 T) NMR spectrometer, using a 3.2 mm HXY probe, tuned to ^{1}H (850.29 MHz), ^{27}Al (221.56 MHz), and ^{17}O (115.27 MHz), and spinning at 24 kHz. DFS excitation pulses were first applied on ^{27}Al (1 ms pulse of 30 W, with a 600 to 150 kHz sweep). The π/2 and π pulses on ^{27}Al were set to 8.3 and 16.6 μs, respectively (~10 kHz RF). The evolution delay following the π/2 pulse on ^{27}Al was set to 2.5 ms. The π/2 pulses on ^{17}O were set to 8.5 μs (~10 kHz RF). Spinal-64 ^{1}H decoupling (100 kHz RF) was applied throughout the sequence (except during the DFS). The recycle delay was set to 1s, and a total of 10000 scans were acquired for each of the 18 increments of the 2D. ^{17}O and ^{27}Al chemical shifts were referenced using respectively tap water (at 0 ppm) and a 1 mol.L^{-1} solution of aluminum-nitrate (at 0 ppm).

^{1}H{^{17}O} D- and J- HMQC. ^{1}H{^{17}O} HMQC MAS NMR experiments were performed on a Bruker 850MHz (20.0 T) NMR spectrometer, using a 1.3 mm HX probe, tuned to ^{1}H (850.29 MHz) and ^{17}O (115.27 MHz), and spinning at 60 kHz. The π/2 and π pulses on ^{1}H were set to 2.05 and 4.1 μs, respectively. The π/2 pulses on ^{17}O were set to 6.0 μs. For the J-HMQC experiment, the evolution delay following the π/2 pulse on ^{1}H was set to 600 μs. For the D-HMQC experiment, the recoupling time τ_{rec} was set to 100 or 300 μs, during which an $SR4^2_1$ pulse was applied on ^{1}H (120 kHz RF) and a WURST pulse was applied on ^{17}O (at an offset of 120 kHz).[66] The recycle delay was set to 0.5s. The number of scans and duration of each experiment can be found in supporting information (Table S1). ^{17}O and ^{1}H chemical shifts were referenced using respectively tap water (at 0 ppm) and a dipeptide (Asp-Ala), for which the low frequency signal was set to 1.1 ppm with respect to tetramethylsilane.

^{17}O MQMAS. A ^{17}O MQMAS experiment was performed on an enriched alumina phase on the SCH-instrument in Tallahassee,[64] using a 3.2 mm single-channel MAS probe, and spinning at 16 kHz. ^{17}O

excitation and conversion pulses were respectively set to 4 and 1.4 µs (600W power), and followed by a 4.4 µs pulse (36W power). The recycle delay was set to 0.2s, and a total of 240 scans were acquired for each of the increments of the 2D. ^{17}O chemical shifts were referenced externally to D_2O at –2.7 ppm (which was measured to be equivalent to tap-water at 0 ppm).

^{17}O DNP. The MAS-DNP experiments were carried out on the 600 MHz/395 GHz setup installed at the National High Magnetic Field Laboratory in Tallahassee. The magnetic field was set at 14.094 T, the gyrotron generates a microwave power of 12 W at the probe base and a frequency of 395.166 GHz. The sample was packed in a 3.2 mm thin wall ZrO_2 rotor and spun at 13 kHz. The temperature for VT/Bearing/Drive were 91.6/98/110 K, leading to a sample temperature under microwave irradiation of ~ 100K, and ~94K in absence of it.[38] The higher drive temperature allowed achieving 13 kHz spinning frequency while reducing the pressure needed. The sample was pre-spun at room temperature with a benchtop spinner (home-built) and the EPR measurement was carried out prior to the MAS-DNP experiment. Finally, 3 freeze-thaw were applied to the sample before insertion into the probe. The powder was impregnated with a 16 mM solution of TEKPol (purchased from Cortecnet) in D_2-tetrachloroethane (Cortecnet) for Al_2O_3, or tetrabromoethane (Sigma-Aldrich) for TiO_2. For the experiments, ~30 mg of powder was impregnated with ~30 µL of solution leading to tooth-pasty texture. The NMR acquisition parameters used for each spectrum are reported in Table S1, for the $^{17}O\{^1H\}$ CPMAS and DFS-echo experiments performed with or without microwaves.

Acknowledgements

This project has received funding from the European Research Council (ERC) under the European Union's Horizon 2020 research and innovation program (grant agreement No 772204; 2017 ERC-COG, MISOTOP project). A portion of this work was performed at the National High Magnetic Field Laboratory, which is supported by the National Science Foundation Cooperative Agreement No. DMR-1644779, the State of Florida and the United States Department of Energy. The MAS-DNP system at the NHMFL is funded in part by NIH S10 OD018519 and P41 GM122698. Financial support from the IR-RMN-THC Fr3050 CNRS for conducting part of the high-field NMR experiments is gratefully acknowledged. The UK 850 MHz solid-state NMR Facility used in this research was funded by EPSRC and BBSRC, as well as the University of Warwick including via part funding through Birmingham Science City Advanced Materials Projects 1 and 2 supported by Advantage West Midlands (AWM) and the European Regional Development Fund (ERDF). Dr Franck Fayon (CEMHTI, CNRS) and Dr Dinu Iuga (University of Warwick) are acknowledged for discussions, and Anastasia Kuznetsova for the BM-enrichment of some of the alumina phases studied here.

Author contributions

C.-H. C., E. G., R. B., B. R., T.-X. M. and D.L. participated to the synthesis and characterization of the enriched-materials. C.-H. C., Ph. G., B. A. and D. L. performed SSNMR analyses at 14.1T. F. M.-V. carried out all DNP experiments. K. C., Z. G., P. F., C. B., M. E. S., B. A. and D. L. participated to the ultra-high field NMR experiments. C.-H. C., T.-X. M., B. A. and D. L. designed the investigations, and D. L. coordinated the project. All co-authors participated in the writing of the manuscript.

Supporting information

Preliminary study on the synthesis of ^{17}O-enriched Li_2*O (including Fig. S1); SEM, N_2 adsorption/desorption isotherms and EDXS analyses of SiO_2 (Fig. S2), Al_2O_3 (Fig. S3), TiO_2 (Fig. S4) and ZrO_2 (Fig. S5); ^{17}O MAS NMR spectra of enriched Zr*O_2 and of the empty zirconia rotor (Fig. S6a), and ^{17}O MAS NMR spectrum of a non-labeled Al_2O_3 phase (Fig. S6b); Fit of the ^{17}O MAS NMR spectrum of enriched Si*O_2, recovered after 1h BM (Fig. S7); ^{27}Al MAS and ^{27}Al{^{1}H} CPMAS NMR analyses of Al_2O_3 phases, before and after enrichment (Fig. S8); Fits of ^{17}O MAS NMR spectra of enriched Al_2*O_3, after different milling times (Fig. S9); Fast MAS ^{1}H NMR spectra of enriched Al_2*O_3, and comparison to the rotor ^{1}H background signal (Fig. S10); ^{17}O DNP and ^{17}O{^{1}H} CP-DNP MAS NMR spectra of enriched Al_2*O_3 (Fig. S11); ^{17}O MAS and ^{17}O{^{1}H} CP MAS NMR spectra of enriched Al_2*O_3 (Fig. S12); Fit of the ^{17}O MAS NMR spectrum of enriched Si*O_2, recovered after 1min BM (Fig. S13); Analysis of the siloxane region of ^{17}O MAS NMR spectra of SiO_2/TiO_2 mixtures labeled using different procedures (Fig. S14); ^{17}O MAS NMR spectra of zirconia phases of different initial crystallinity, recovered after 1h BM (Fig. S15); ^{17}O MAS NMR spectra of enriched alumina and titania, after heat-treatment at 900°C (Fig. S16); ^{17}O NMR parameters used for the acquisition of the NMR spectra (Table S1).

References

1. Ashbrook, S. E.; Smith, M. E., Solid state ^{17}O NMR—an introduction to the background principles and applications to inorganic materials. *Chem. Soc. Rev.* **2006,** *35*, 718-735.
2. Huo, H.; Peng, L.; Gan, Z.; Grey, C. P., Solid-State MAS NMR Studies of Brønsted Acid Sites in Zeolite H-Mordenite. *J. Am. Chem. Soc.* **2012,** *134*, 9708-9720.
3. Bignami, G. P. M.; Davis, Z. H.; Dawson, D. M.; Morris, S. A.; Russell, S. E.; McKay, D.; Parke, R. E.; Iuga, D.; Morris, R. E.; Ashbrook, S. E., Cost-effective ^{17}O enrichment and NMR spectroscopy of mixed-metal terephthalate metal–organic frameworks. *Chem. Sci.* **2018,** *9*, 850-859.
4. Bignami, G. P. M.; Dawson, D. M.; Seymour, V. R.; Wheatley, P. S.; Morris, R. E.; Ashbrook, S. E., Synthesis, Isotopic Enrichment, and Solid-State NMR Characterization of Zeolites Derived from the Assembly, Disassembly, Organization, Reassembly Process. *J. Am. Chem. Soc.* **2017,** *139*, 5140-5148.
5. Heard, C. J.; Grajciar, L.; Rice, C. M.; Pugh, S. M.; Nachtigall, P.; Ashbrook, S. E.; Morris, R. E., Fast room temperature lability of aluminosilicate zeolites. *Nature Comm.* **2019,** *10*, 4690.
6. Reeves, P. J.; Seymour, I. D.; Griffith, K. J.; Grey, C. P., Characterizing the Structure and Phase Transition of Li_2RuO_3 Using Variable-Temperature ^{17}O and ^{7}Li NMR Spectroscopy. *Chem. Mater.* **2019,** *31*, 2814-2821.
7. Geng, F.; Shen, M.; Hu, B.; Liu, Y.; Zeng, L.; Hu, B., Monitoring the evolution of local oxygen environments during $LiCoO_2$ charging via ex situ ^{17}O NMR. *Chem. Comm.* **2019,** *55*, 7550-7553.
8. Hope, M. A.; Halat, D. M.; Magusin, P. C. M. M.; Paul, S.; Peng, L.; Grey, C. P., Surface-selective direct ^{17}O DNP NMR of CeO_2 nanoparticles. *Chem. Comm.* **2017,** *53*, 2142-2145.
9. Li, Y.; Wu, X.-P.; Jiang, N.; Lin, M.; Shen, L.; Sun, H.; Wang, Y.; Wang, M.; Ke, X.; Yu, Z.; Gao, F.; Dong, L.; Guo, X.; Hou, W.; Ding, W.; Gong, X.-Q.; Grey, C. P.; Peng, L., Distinguishing faceted oxide nanocrystals with ^{17}O solid-state NMR spectroscopy. *Nature Comm.* **2017,** *8*, 581.
10. Shen, L.; Wu, X.-P.; Wang, Y.; Wang, M.; Chen, J.; Li, Y.; Huo, H.; Hou, W.; Ding, W.; Gong, X.-Q.; Peng, L., ^{17}O Solid-State NMR Studies of ZrO_2 Nanoparticles. *J. Phys. Chem. C*, **2019,** *123*, 4158-4167.
11. Chen, J.; Wu, X.-P.; Hope, M. A.; Qian, K.; Halat, D. M.; Liu, T.; Li, Y.; Shen, L.; Ke, X.; Wen, Y.; Du, J.-H.; Magusin, P. C. M. M.; Paul, S.; Ding, W.; Gong, X.-Q.; Grey, C. P.; Peng, L., Polar surface structure of oxide nanocrystals revealed with solid-state NMR spectroscopy. *Nature Comm.* **2019,** *10*, 5420.
12. MacKenzie, K. J. D.; Smith, M. E., Multinuclear Solid-State Nuclear Magnetic Resonance of Inorganic Materials, Pergamon: **2002**; *Chapter 6*.
13. Jaworski, A.; Stevensson, B.; Edén, M., Direct ^{17}O NMR experimental evidence for Al–NBO bonds in Si-rich and highly polymerized aluminosilicate glasses. *Phys. Chem. Chem. Phys.* **2015,** *17*, 18269-18272.
14. Bastow, T. J.; Smith, M. E.; Whitfield, H. J., Characterisation of zirconia gels by ^{17}O nuclear magnetic resonance. *J. Mater. Chem.* **1992,** *2*, 989-990.
15. Bastow, T. J.; Moodie, A. F.; Smith, M. E.; Whitfield, H. J., Characterisation of titania gels by ^{17}O nuclear magnetic resonance and electron diffraction. *J. Mater. Chem.* **1993,** *3*, 697-702.
16. Babonneau, F.; Bonhomme, C.; Gervais, C.; Maquet, J., Advances in Characterisation Methods for Sol-Gel Derived Materials: High Resolution Solid State Nuclear Magnetic Resonance. *J. Sol-Gel Sci. Technol.* **2004,** *31*, 9-17.
17. Griffin, J. M.; Clark, L.; Seymour, V. R.; Aldous, D. W.; Dawson, D. M.; Iuga, D.; Morris, R. E.; Ashbrook, S. E., Ionothermal ^{17}O enrichment of oxides using microlitre quantities of labelled water. *Chem. Sci.* **2012,** *3*, 2293-2300.
18. Métro, T.-X.; Gervais, C.; Martinez, A.; Bonhomme, C.; Laurencin, D., Unleashing the Potential of ^{17}O NMR Spectroscopy Using Mechanochemistry. *Angew. Chem.* **2017,** *129*, 6907-6911.
19. James, S. L.; Adams, C. J.; Bolm, C.; Braga, D.; Collier, P.; Friščić, T.; Grepioni, F.; Harris, K. D. M.; Hyett, G.; Jones, W.; Krebs, A.; Mack, J.; Maini, L.; Orpen, A. G.; Parkin, I. P.; Shearouse, W. C.; Steed, J. W.; Waddell, D. C., Mechanochemistry: opportunities for new and cleaner synthesis. *Chem. Soc. Rev.* **2012,** *41*, 413-447.
20. Friščić, T.; Mottillo, C.; Titi, H. M., Mechanochemistry for Synthesis. *Angew. Chem.* **2019,** doi: 10.1002/anie.201906755.
21. Bowmaker, G. A., Solvent-assisted mechanochemistry. *Chem. Comm.* **2013,** *49*, 334-348.
22. Leskes, M.; Moore, A. J.; Goward, G. R.; Grey, C. P., Monitoring the Electrochemical Processes in the Lithium–Air Battery by Solid State NMR Spectroscopy. *J. Phys. Chem. C*, **2013,** *117*, 26929-26939.
23. Abys, J. A.; Barnes, D. M.; Feller, S.; Rouse, G. B.; Risen, W. M., Preparation of O^{17}-labelled glasses and glass precursers. *Mater. Res. Bull.* **1980,** *15*, 1581-1587.
24. Merle, N.; Trébosc, J.; Baudouin, A.; Rosal, I. D.; Maron, L.; Szeto, K.; Genelot, M.; Mortreux, A.; Taoufik, M.; Delevoye, L.; Gauvin, R. M., ^{17}O NMR Gives Unprecedented Insights into the Structure of Supported Catalysts and Their Interaction with the Silica Carrier. *J. Am. Chem. Soc.* **2012,** *134*, 9263-9275.

25. Freude, D.; Haase, J., Survey of NMR Parameters for Quadrupolar Nuclei in Powder Materials, in Particular for ^{27}Al, ^{23}Na and ^{17}O. http://www.quad-nmr.de, **2019**.
26. Walter, T. H.; Oldfield, E., Magic angle spinning oxygen-17 NMR of aluminum oxides and hydroxides. *J. Phys. Chem.* **1989,** *93*, 6744-6751.
27. Bastow, T. J.; Stuart, S. N., ^{17}O NMR in simple oxides. *Chem. Phys.* **1990,** *143*, 459-467.
28. Sun, X.; Dyballa, M.; Yan, J.; Li, L.; Guan, N.; Hunger, M., Solid-state NMR investigation of the $^{16/17}$O isotope exchange of oxygen species in pure-anatase and mixed-phase TiO_2. *Chem. Phys. Lett.* **2014,** *594*, 34-40.
29. Pimentel, H. R. X.; Aguiar, D. L. M.; San Gil, R. A. S.; Souza, E. F.; Ferreira, A. R.; Leitão, A. A.; Alencastro, R. B.; Menezes, S. M. C.; Chiaro, S. S. X., ^{17}O MAS NMR and first principles calculations of ZrO_2 polymorphs. *Chem. Phys. Lett.* **2013,** *555*, 96-100.
30. Li, W.; Wang, Q.; Xu, J.; Aussenac, F.; Qi, G.; Zhao, X.; Gao, P.; Wang, C.; Deng, F., Probing the surface of γ-Al_2O_3 by oxygen-17 dynamic nuclear polarization enhanced solid-state NMR spectroscopy. *Phys. Chem. Chem. Phys.* **2018,** *20*, 17218-17225.
31. Oglesby, J. V.; Zhao, P.; Stebbins, J. F., Oxygen sites in hydrous aluminosilicate glasses: the role of Al-O-Al and H_2O. *Geochim. Cosmochim. Acta*, **2002,** *66*, 291-301.
32. Neuhoff, P. S.; Zhao, P.; Stebbins, J. F., Effect of extraframework species on ^{17}O NMR chemical shifts in zeolite A. *Micropor. Mesopor. Mater.* **2002,** *55*, 239-251.
33. Frydman, L.; Harwood, J. S., Isotropic Spectra of Half-Integer Quadrupolar Spins from Bidimensional Magic-Angle Spinning NMR. *J. Am. Chem. Soc.* **1995,** *117*, 5367-5368.
34. Batista, A. T. F.; Wisser, D.; Pigeon, T.; Gajan, D.; Diehl, F.; Rivallan, M.; Catita, L.; Gay, A.-S.; Lesage, A.; Chizallet, C.; Raybaud, P., Beyond γ-Al_2O_3 crystallite surfaces: The hidden features of edges revealed by solid-state ^{1}H NMR and DFT calculations. *J. Catal.* **2019,** *378*, 140-143.
35. Pourpoint, F.; Gervais, C.; Bonhomme-Coury, L.; Azaïs, T.; Coelho, C.; Mauri, F.; Alonso, B.; Babonneau, F.; Bonhomme, C., Calcium Phosphates and Hydroxyapatite: Solid-State NMR Experiments and First-Principles Calculations. *Appl. Magn. Reson.* **2007,** *32*, 435-457.
36. Taoufik, M.; Szeto, K. C.; Merle, N.; Rosal, I. D.; Maron, L.; Trébosc, J.; Tricot, G.; Gauvin, R. M.; Delevoye, L., Heteronuclear NMR Spectroscopy as a Surface-Selective Technique: A Unique Look at the Hydroxyl Groups of γ-Alumina. *Chem. - Eur. J.* **2014,** *20*, 4038-4046.
37. Digne, M.; Raybaud, P.; Sautet, P.; Guillaume, D.; Toulhoat, H., Atomic Scale Insights on Chlorinated γ-Alumina Surfaces. *J. Am. Chem. Soc.* **2008,** *130*, 11030-11039.
38. Rossini, A. J.; Zagdoun, A.; Lelli, M.; Lesage, A.; Copéret, C.; Emsley, L. Dynamic Nuclear Polarization Surface Enhanced NMR Spectroscopy. *Acc. Chem. Res.* **2013**, *46*, 1942-1951.
39. Lesage, A.; Lelli, M.; Gajan, D.; Caporini, M. A.; Vitzthum, V.; Miéville, P.; Alauzun, J.; Roussey, A.; Thieuleux, C.; Mehdi, A.; Bodenhausen, G.; Coperet, C.; Emsley, L., Surface Enhanced NMR Spectroscopy by Dynamic Nuclear Polarization. *J. Am. Chem. Soc.* **2010,** *132*, 15459-15461.
40. Scolan, E.; Magnenet, C.; Massiot, D.; Sanchez, C., Surface and bulk characterisation of titanium–oxo clusters and nanosized titania particles through ^{17}O solid state NMR. *J. Mater. Chem.* **1999,** *9*, 2467-2474.
41. Blanchard, J.; Bonhomme, C.; Maquet, J.; Sanchez, C., Characterisation of sol–gel derived titanium oxopolymers: first evidence of Ti–OH groups through ^{1}H–^{17}O CP NMR experiments. *J. Mater. Chem.* **1998,** *8*, 985-989.
42. Shi, Y.; Sun, H.; Saidi, W. A.; Nguyen, M. C.; Wang, C. Z.; Ho, K.; Yang, J.; Zhao, J., Role of Surface Stress on the Reactivity of Anatase TiO_2(001). *J. Phys. Chem. Lett.* **2017,** *8*, 1764-1771.
43. Aschauer, U.; He, Y.; Cheng, H.; Li, S.-C.; Diebold, U.; Selloni, A., Influence of Subsurface Defects on the Surface Reactivity of TiO_2: Water on Anatase (101). *J. Phys. Chem. C*, **2010,** *114*, 1278-1284.
44. Tielens, F.; Gervais, C.; Deroy, G.; Jaber, M.; Stievano, L.; Coelho Diogo, C.; Lambert, J.-F., Characterization of Phosphate Species on Hydrated Anatase TiO_2 Surfaces. *Langmuir* **2016,** *32*, 997-1008.
45. Walter, T. H.; Turner, G. L.; Oldfield, E., Oxygen-17 cross-polarization nmr spectroscopy of inorganic solids. *J. Magn. Reson.* **1988,** *76*, 106-120.
46. Gervais, C.; Babonneau, F.; Smith, M. E., Detection, Quantification, and Magnetic Field Dependence of Solid-State ^{17}O NMR of X−O−Y (X,Y = Si,Ti) Linkages: Implications for Characterizing Amorphous Titania-Silica−Based Materials. *J. Phys. Chem. B*, **2001,** *105*, 1971-1977.
47. Gervais, C.; Babonneau, F.; Hoebbel, D.; Smith, M. E., Solid State NMR Interaction Parameters of Oxygens Linking Titanium and Silicon in Crystalline Cyclic Titanodiphenylsiloxanes. *Solid St. Nucl. Magn. Reson.* **2000,** *17*, 2-14.
48. Frank, O.; Zukalova, M.; Laskova, B.; Kürti, J.; Koltai, J.; Kavan, L., Raman spectra of titanium dioxide (anatase, rutile) with identified oxygen isotopes (16, 17, 18). *Phys. Chem. Chem. Phys.* **2012,** *14*, 14567-14572.
49. Brezová, V.; Barbieriková, Z.; Zukalová, M.; Dvoranová, D.; Kavan, L., EPR study of ^{17}O-enriched titania nanopowders under UV irradiation. *Catal. Today*, **2014,** *230*, 112-118.

50. Clark, T. M.; Grandinetti, P. J.; Florian, P.; Stebbins, J. F., An ^{17}O NMR Investigation of Crystalline Sodium Metasilicate: Implications for the Determination of Local Structure in Alkali Silicates. *J. Phys. Chem. B*, **2001,** *105*, 12257-12265.
51. Larsen, F. H.; Rossano, S.; Farnan, I., Order and Disorder in Titanosilicate Glass by ^{17}O MAS, off-MAS, and 3Q-QCPMG-MAS Solid-State NMR. *J. Phys. Chem. B*, **2007,** *111*, 8014-8019.
52. Yang, S.; Park, K. D.; Oldfield, E., Oxygen-17 labeling of oxides and zeolites. *J. Am. Chem. Soc.* **1989,** *111*, 7278-7279.
53. Boldyreva, E., Mechanochemistry of inorganic and organic systems: what is similar, what is different? *Chem. Soc. Rev.* **2013,** *42*, 7719-7738.
54. Hutchings, B. P.; Crawford, D. E.; Gao, L.; Hu, P.; James, S. L., Feedback Kinetics in Mechanochemistry: The Importance of Cohesive States. *Angew. Chem.* **2017,** *56*, 15252-15256.
55. Kulla, H.; Haferkamp, S.; Akhmetova, I.; Röllig, M.; Maierhofer, C.; Rademann, K.; Emmerling, F., In Situ Investigations of Mechanochemical One-Pot Syntheses. *Angew. Chem.* **2018,** *57*, 5930-5933.
56. Xu, Y.; Champion, L.; Gabidullin, B.; Bryce, D. L., A kinetic study of mechanochemical halogen bond formation by in situ ^{31}P solid-state NMR spectroscopy. *Chem. Comm.* **2017,** *53*, 9930-9933.
57. Michalchuk, A. A. L.; Tumanov, I. A.; Konar, S.; Kimber, S. A. J.; Pulham, C. R.; Boldyreva, E. V., Challenges of Mechanochemistry: Is In Situ Real-Time Quantitative Phase Analysis Always Reliable? A Case Study of Organic Salt Formation. *Advanced Sci.* **2017,** *4*, 1700132.
58. Užarević, K.; Halasz, I.; Friščić, T., Real-Time and In Situ Monitoring of Mechanochemical Reactions: A New Playground for All Chemists. *J. Phys. Chem. Lett.* **2015,** *6*, 4129-4140.
59. Michalchuk, A. A. L.; Tumanov, I. A.; Boldyreva, E. V., Ball size or ball mass – what matters in organic mechanochemical synthesis? *CrystEngComm* **2019,** *21*, 2174-2179.
60. Belenguer, A. M.; Michalchuk, A. A. L.; Lampronti, G. I.; Sanders, J. K. M., Understanding the unexpected effect of frequency on the kinetics of a covalent reaction under ball-milling conditions. *Beilstein J. Org. Chem.* **2019,** *15*, 1226-1235.
61. Gotor, F. J.; Achimovicova, M.; Real, C.; Balaz, P., Influence of the milling parameters on the mechanical work intensity in planetary mills. *Powder Technol.* **2013,** *233*, 1-7.
62. Kulla, H.; Fischer, F.; Benemann, S.; Rademann, K.; Emmerling, F., The effect of the ball to reactant ratio on mechanochemical reaction times studied by in situ PXRD. *CrystEngComm* **2017,** *19*, 3902-3907.
63. Zagdoun, A.; Casano, G.; Ouari, O.; Schwarzwälder, M.; Rossini, A. J.; Aussenac, F.; Yulikov, M.; Jeschke, G.; Copéret, C.; Lesage, A.; Tordo, P.; Emsley, L., Large Molecular Weight Nitroxide Biradicals Providing Efficient Dynamic Nuclear Polarization at Temperatures up to 200 K. *J. Am. Chem. Soc.* **2013,** *135*, 12790-12797.
64. Gan, Z.; Hung, I.; Wang, X.; Paulino, J.; Wu, G.; Litvak, I. M.; Gor'kov, P. L.; Brey, W. W.; Lendi, P.; Schiano, J. L.; Bird, M. D.; Dixon, I. R.; Toth, J.; Boebinger, G. S.; Cross, T. A., NMR spectroscopy up to 35.2T using a series-connected hybrid magnet. *J. Magn. Reson.* **2017,** *284*, 125-136.
65. Perras, F. A.; Viger-Gravel, J.; Burgess, K. M. N.; Bryce, D. L., Signal enhancement in solid-state NMR of quadrupolar nuclei. *Solid St. Nucl. Magn. Reson.* **2013,** *51-52*, 1-15.
66. Brinkmann, A.; Kentgens, A. P. M. Proton-Selective ^{17}O–^{1}H Distance Measurements in Fast Magic-Angle-Spinning Solid-State NMR Spectroscopy for the Determination of Hydrogen Bond Lengths. *J. Am. Chem. Soc.* **2006**, *128*, 14758-14759.

For Table of contents only

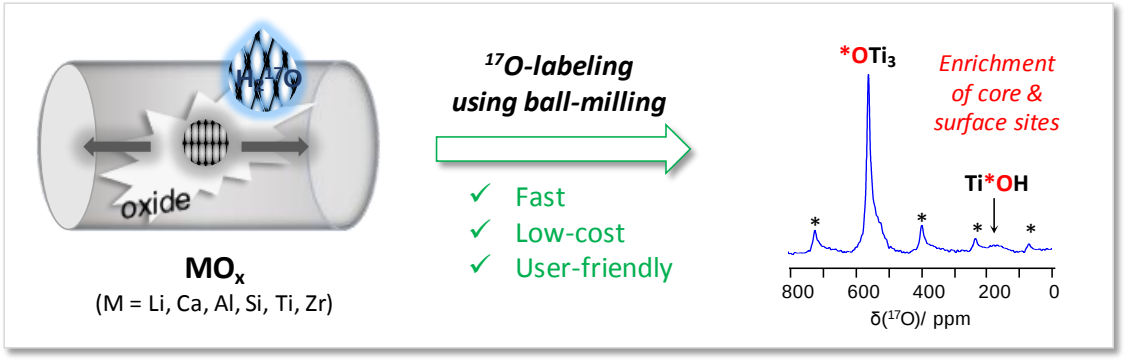

The direct ^{17}O-enrichment of s-, p- and d- block metal oxides is achieved with high efficiency using mechanochemistry. Atomic-level insight into the enrichment process is obtained using high-resolution ^{17}O solid state NMR and DNP analyses, which demonstrate that enriched oxygen sites are present both at the surface and within the oxide particles. Moreover, it is demonstrated how these labeling schemes allow studying unique aspects of mechanochemical reactions between oxides by ^{17}O NMR.